Acta Pharmaceutica Sinica B 2024;14(3):1077−1097

Chinese Pharmaceutical Association
Institute of Materia Medica, Chinese Academy of Medical Sciences

Acta Pharmaceutica Sinica B

www.elsevier.com/locate/apsb
www.sciencedirect.com

REVIEW

Design consideration of phthalocyanines as sensitizers for enhanced sono-photodynamic combinatorial therapy of cancer

Lindokuhle Cindy Nene, Heidi Abrahamse*

Laser Research Centre, Faculty of Health Sciences, University of Johannesburg, Doornfontein 2028, South Africa

Received 26 July 2023; received in revised form 8 October 2023; accepted 25 November 2023

KEY WORDS

Sonodynamic therapy;
Photodynamic therapy;
Combinatorial therapy;
Phthalocyanines;
Sensitizer;
Cancer

Abstract Cancer remains one of the diseases with the highest incidence and mortality globally. Conventional treatment modalities have demonstrated threatening drawbacks including invasiveness, non-controllability, and development of resistance for some, including chemotherapy, radiation, and surgery. Sono-photodynamic combinatorial therapy (SPDT) has been developed as an alternative treatment modality which offers a non-invasive and controllable therapeutic approach. SPDT combines the mechanism of action of sonodynamic therapy (SDT), which uses ultrasound, and photodynamic therapy (PDT), which uses light, to activate a sensitizer and initiate cancer eradication. The use of phthalocyanines (Pcs) as sensitizers for SPDT is gaining interest owing to their ability to induce intracellular oxidative stress and initiate toxicity under SDT and PDT. This review discusses some of the structural prerequisites of Pcs which may influence their overall SPDT activities in cancer therapy.

*Corresponding author.
E-mail address: habrahamse@uj.ac.za (Heidi Abrahamse).

Peer review under the responsibility of Chinese Pharmaceutical Association and Institute of Materia Medica, Chinese Academy of Medical Sciences.

https://doi.org/10.1016/j.apsb.2023.11.030

1. Introduction

Photodynamic therapy (PDT) and sonodynamic therapy (SDT) are cancer treatment modalities developed as alternatives to the conventional chemotherapy, surgery, or radiation[1,2]. These modalities are mainly developed to address the inherent limitation observed with the conventional cancer therapeutic techniques, such as invasiveness and resistance[3–5]. Current studies focus on developing PDT and SDT as monotherapies or in combination, as sono-photodynamic combinatorial therapy (SPDT). The techniques each involve the synergistic activities of three key components, including a non-toxic sensitizer, light of specific wavelength (in PDT)[6] or low frequency ultrasound (in SDT)[7] and molecular oxygen (O_2) to initiate cytotoxicity[8]. Both treatment modalities offer controllable and minimally invasive techniques for cancer therapy and can potentially treat a wider-range of cancer types[9–11]. A plethora of sensitizers have been designed and studied for SDT/SPDT of cancers including porphyrins, chlorins, xanthenes and phthalocyanine to mention a few[4,12,13]. Phthalocyanines (Pcs) are regarded as the second generation of sensitizers for PDT and have shown promising results as anticancer agents[14,15]. The main interest on Pcs for SPDT compared to other sensitizers is owed to their maximum absorption within the near-infrared region (NIR) of the electromagnetic spectrum. The use of light of wavelengths within the NIR is better suited for PDT/SPDT treatments of cancers as it offers improved tissue penetrability compared to shorter wavelengths (with porphyrins and chlorins)[12]. Additionally, Pcs are generally stable under physiological conditions and structurally relatively easier to modify to tailor their physicochemical properties (including addition of various central metals or substituents)[15,16]. The general structures of Pcs are shown in Fig. 1.

Pcs are macrocycles comprised of tetra-pyrrolic subunits with a central cavity in which a metal ion or metalloid may be chelated to yield metallated Pcs from free base Pcs (H_2Pcs) (Fig. 1)[16–18]. Their structures are further modified through the addition of R-groups on different positions. Pcs are electron-rich with an 18-π electron conjugated system which affords them impressive electronic and physicochemical properties[19,20].

This review will focus on Pcs as sensitizers for SDT and SPDT. For PDT a wide range of Pcs with varying physical and chemical properties have been studied and are well reported in the literature[21,22]. It is important to maintain these properties when intending to apply Pcs for combinatorial therapies such as SPDT to ensure effective photo-activities. The structural variations of Pcs in SDT have been reported to a lesser extent compared to PDT. A substantial number of review articles have looked at the general library of sensitizers for SDT. Various Pcs designs have been reported and studied on their SDT and SPDT anticancer activities. This review will discuss for the first time some of the factors affecting the sono-activities of Pcs for cancer treatments in terms of their structural designs to possibly postulate the design consideration of Pcs for SDT and SPDT.

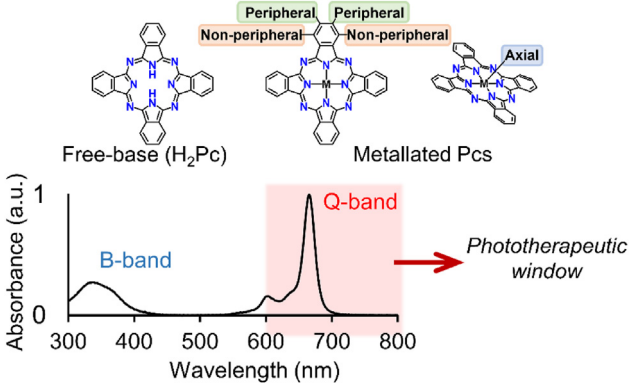

Figure 1 The general structures of unmetallated free-base and metallated Pcs structures showing the peripheral (α), non-peripheral (β) and axial R-group points. And the typical UV−Vis spectra of Pcs showing the distinctive Q- and B-bands, and the phototherapeutic window.

2. Rationale for use of Pcs in SPDT

Pcs have gained much interest as sensitizers for PDT for various reasons including their impressive electronic properties and increased light absorption in the NIR[12,23,24]. The extinction coefficients of Pcs in the NIR are relatively high ($>10^5$ L/(mol·cm))[25]. This is beneficial as increased light wavelength allows for deeper tissue penetrability compared to lower wavelengths[24,26]. Moreover, biological molecules show absorption outside the 600−800 nm range[27,28]. This region is known as the therapeutic window and competition for photon-energy is reduced at this wavelength range. A typical UV−Vis absorption spectrum of Pcs shows an intense absorption peak at wavelengths between 600 and 850 nm, this peak is denoted the Q-band (Fig. 1)[29,30]. A lower absorption intensity in the blue region is also evident for Pcs and is denoted as the B-band[30]. For PDT, Pcs are typically excited using light of wavelengths corresponding to the wavelength of their Q-bands. Furthermore, Pcs have shown minimal dark toxicity and impressive photo-activities during PDT[24]. Although Pcs-mediated PDT seems promising, light penetrability into tissue is only limited to ~10 mm past the epidermis, even at longer NIR wavelengths[11,31]. Therefore, PDT alone is only limited to the efficient eradication of superficial tumours[32]. To address this issue, SDT has been considered and developed as an alternative or supplementary treatment modality to PDT. The degree of light penetrability past the epidermis compared to ultrasound for cancer treatment is shown in Fig. 2.

SDT utilizes low-frequency ultrasound which may be focused on a narrow region, and therefore maintaining a controllable therapy[33,34]. The ultrasound used in SDT has a low tissue attenuation coefficient and may traverse tissue relatively deeper compared to light[35] (Fig. 2). Skin and prostate cancers are easily reachable by NIR light alone and may be treated by PDT. It is more challenging to eradicate cancers located in deep tissues such as liver, stomach, cervical and bone cancers, as well as treating metastatic cancers. These may therefore be reachable by ultrasound in SDT or SPDT[36]. Pcs have shown synergistic activities with ultrasound to initiate cytotoxicity in various cancer cell models[5,12]. Moreover, Pcs have shown the ability to respond to both ultrasound and light in SPDT and therefore enables the use of a single sensitizer for this treatment modality making Pcs generally interesting as SPDT agents[2].

3. Mechanism of action of Pcs in SPDT

Combination therapy is a common tool for increasing the therapeutic efficacies of different treatment modalities. This type of treatment involves the synergistic therapeutic activities of two or more modalities for the treatment of specific diseases. The

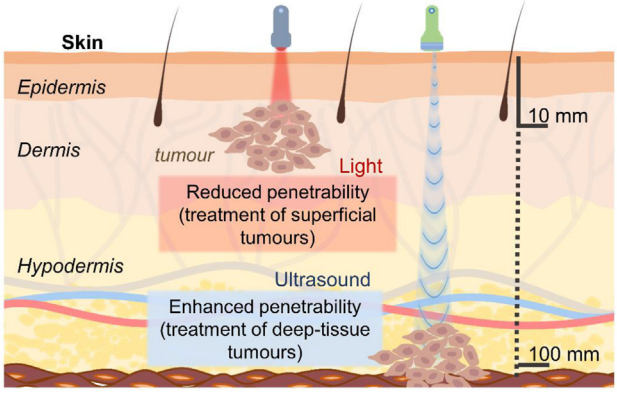

Figure 2 The tissue penetrability of light is limited and only reaches slightly into the dermis. Ultrasound shows improved penetrability into tissue past the hypodermis to reach deep tissue seated tumours.

mechanisms of action of Pcs sensitizers under light and ultrasound exposure to elicit tumouricidal effects involve different processes which may overlap to an extent. The mechanism of action involved in SPDT is shown in Fig. 3.

3.1. *Mechanism of action in PDT*

The mechanism of action in PDT is well-known and has been defined using the Jablonski diagram[22,37]. The diagram outlines the energy pathways from the photo-activated Pcs to the generation of the cytotoxic reactive oxygen species (ROS) (Fig. 3). Briefly, the non-toxic Pcs in the ground state (S_0) absorb photon-energy from the light to which they are exposed to occupy the excited energy states (S_1)[38]. The excited Pcs may relax back to the ground state through fluorescence or undergo internal conversion, resulting in the non-radiative relaxation to release heat[39]. This is known as photo-thermal conversion. Alternatively, the excited Pcs may undergo intersystem crossing (ISC) and occupy the triplet excited state (T_1). The Pcs in the T_1 may therefore initiate ROS-generating processes through two main routes, namely, the type I and the type II before returning to the S_0[40]. The type I involves the transfer of an electron (e^-) from the excited Pcs to a biomolecular-substrates in the cells to yield ROS such as hydrogen peroxide (H_2O_2), superoxide ($O_2^{-\cdot}$) or hydroxyl ($OH\cdot$) radicals, Fig. 3. The type II route involves the transfer of energy from the excited Pcs in the T_1 to nearby molecular oxygen (O_2) to yield singlet oxygen ($^1O_2$) ROS (Fig. 3). For Pcs, the type II route been defined as the predominant ROS-generation process in PDT using Pcs.

3.2. *Mechanism of action in SDT*

In SDT, the mechanism of action is not yet clear. However, possible mechanisms of action have been proposed in the literature. The current proposition is explained through a phenomenon referred to as acoustic cavitation[33,41,42]. Acoustic cavitation can be classified into two types, namely: inertial and stable (non-inertial) cavitation (Fig. 3).

3.2.1. *Inertial cavitation*

Inertial cavitation involves the nucleation, growth, and violent jetting of gas-filled microbubbles[43–45]. The bursting bubbles may emit light known as sono-luminescence which causes nearby Pcs to be activated similarly to PDT to yield ROS. The emission intensities of the sonoluminescence were reported to be within the wavelength range of 300–700 nm with maximum emission intensity at 500 nm by Giuntini et al.[46] The ultrasound parameters used in the study were of frequency 1.86 MHz and power of 1.5 W/cm^2 [46]. Sazgarnia et al. observed the sonoluminescence emission wavelengths at ranges 350–450 nm; 450–550 nm and 550–650 nm when using gel phantom-based tissue simulators and ultrasound of 1.1 MHz, 2 W/cm^2 [47]. Furthermore, inertial cavitation may lead to localized increase in temperature (up to ~10,000 K) and pressure (>80 MPa) within the tumour microenvironment[3,48]. This dynamic process promotes water-pyrolysis yielding $\cdot OH$ and H_2O_2; and hyperthermia, resulting in tumour ablation.

3.2.2. *Stable cavitation*

Under stable cavitation, bubbles continuously oscillate within the cells exerting shear forces intracellularly[49,50]. The bubbles eventually burst releasing shock forces resulting in the increase of intracellular pressure and therefore causing damage to the cytoskeleton and eventually lead to necrosis[11,51]. This mechanism of cell death does not involve oxidative stress from ROS yields as in inertial cavitation, instead, cytoskeleton undergoes physical damage as a result of released shock forces from the jetting bubbles. Additionally, the cellular membrane loses its integrity through stable cavitation (formation of pores known as sonoporation), thus, allowing for facile release and internalization of sensitizer molecules for SDT treatment[52]. Plasma membrane poration was observed for US treated MAT B III cells using US frequency of 1.15 MHz[52]. Helfield et al. also reports on the membrane sono-poration of apical and basal cells which results in cellular permeability induced by microbubble oscillation within the cells after US irradiations[50]. From the study, an increase in sono-poration effect was observed at lower frequency ultrasound (0.5 MHz) compared to 1 and 2 MHz[50]. Stable cavitation is known to occur predominantly at low frequency ultrasound[51].

Overall, SDT promotes a destructive effect on the cancer cytoskeleton and biological functions of enzymes and organelles through oxidative and non-oxidative stress.

The coexistence of the mechanisms of both PDT and SDT while using a single sensitizer molecule to illicit cytotoxicity is enabled during SPDT, as shown in Fig. 3. The mechanism of action in SPDT is an important consideration when designing Pcs for this treatment technique.

4. Molecular design considerations of Pcs for SPDT

Generally, Pcs are relatively easily tuneable. Variations to their structures may be introduced using several strategies, including varying the position and type of substituents, varying the central metal or by conjugating the Pcs to different bio-active complexes and nanoparticles. Each of these structural changes results in different physicochemical properties which play a role in the overall sono-photo-therapeutic activities of the Pcs.

4.1. *Effect of central metal*

The use of metals is a common way of enhancing the NIR absorption of Pcs. Generally, closed-shell diamagnetic metals such as Al, Zn, In, Ga etc. have been used for Pcs and are known to promote the T_1 population and ROS yields of Pcs during PDT[39,53]. When targeting photo-thermal therapy, however, open shell

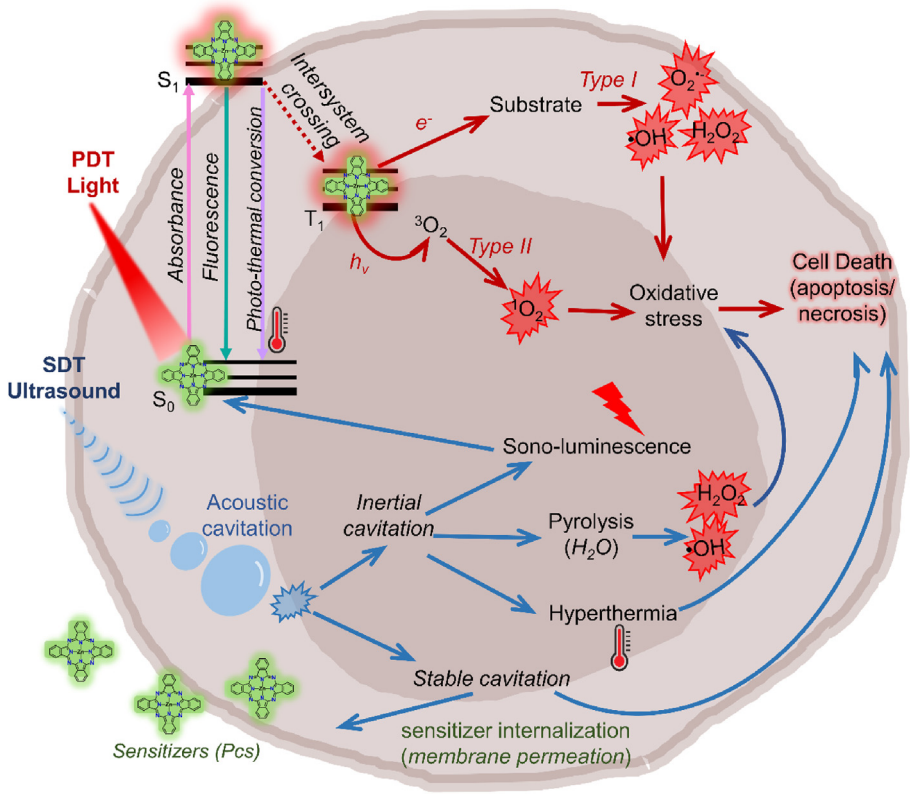

Figure 3 The mechanism of action in SPDT using Pcs for cancer treatment. The light results in the generation of ROS through the type I or type II route. The ultrasound causes inertial cavitation resulting in the emission of sonoluminescence, pyrolysis-mediated ROS yields, and hyperthermia; and stable cavitation which enhances sensitizer internalization and destabilization of cell integrity. All these processes result in cell death.

paramagnetic metals such as Co, Mn, and Fe etc. may be used[39]. These are known to reduce the ISC efficiency and promote photothermal conversion; the ROS yields are reduced when these metals are used[39,54]. The increase in metal sizes has been reported to further enhance T_1 population through a phenomenon known as the heavy atom effect in PDT[55,56]. Various central metals, metalloids, and lanthanide (Ln)-bearing Pcs have been studied in SDT or SPDT and will be discussed herein. The effect of metals on Pcs has been studied to a lesser extent in SDT compared to PDT. A summary of the Pcs structures used in the study of the metal-effect under sono-treatments are shown in Fig. 4.

An improvement in the SDT activities of Pcs by use of central metal compared to their free-base counterparts has been reported in the literature[57,58]. The comparison of the SDT activities of the free-base Pc **1** to the metallated Pc **2** and Pc **3**[57]; and the free-base Pc **4** compared to the metallated Pc **5** and Pc **6**[58]; and finally, Pc **7** compared to Pc **8** and Pc **9**[59] showed that metallated Pcs have enhanced SDT activities compared to the corresponding free-base counterparts. The enhanced SDT activities of the Pcs were seen with increased ROS ($^1O_2$) yields and increase cytotoxicity for some. Therefore, the central metal may play a key role in the SDT efficacies of Pcs. Generally, the Pcs with bigger central metals also showed increased SDT activities *i.e.*, In > Ga[57,59], In > Zn[58]. Considering the increase in efficacies observed for both PDT and SDT when using metallated Pcs compared to free-base Pcs, it may be deduced that in SPDT, metallated Pcs may be favourable. Pd Pc **10**[60] and In Pc **11**[61] have been reported for SDT. The SDT activities were higher for the larger In Pc **11** compared to the smaller Pd Pc **10**. Although the heavy atom effect has been observed and defined for Pcs with larger metals during PDT, for SDT, the increase in activities for Pcs with larger metals is not yet clear. However, it may be related to the increase in nucleation sites for bubbles during acoustic cavitation.

4.2. *Effect of substituents (R-groups)*

The type and positions of the R-groups on the Pcs structures have been shown to alter their overall properties and therapeutics behaviours. Several strategies may be used to vary the addition of R-groups on the Pcs structures. The structures of some of the Pcs with varying R-group properties are shown in Fig. 5.

4.2.1. *Effect of position and number of substituents*

The positions of the R-groups on the Pcs play a key role in their electronic properties. The positions of the R-groups have been reported to influence the Q-band wavelengths. Sindelo et al. reported on the Q-band red-shifting for tetra-morpholine Pcs with R-groups on the α-positions compared to β-positions[62]. The Q-bands of Pcs are influenced by their molecular orbital properties characterized by the energy gap between lowest unoccupied molecular orbital (LUMO) and the highest occupied molecular orbital (HOMO). The α-R-groups are known to cause the destabilization of the HOMO and reduction of the HOMO-LUMO gap and therefore result in red-shifting of the Q-band[63]. Moreover, α-substituted Pcs have been reported to have improved solubility compared to their β-substituted counterparts[64]. This effect has been reported by Ikeuchi et al., comparing anionic water-soluble Pcs with R-groups on the α- and β-positions[61]. Farajzadeh et al.

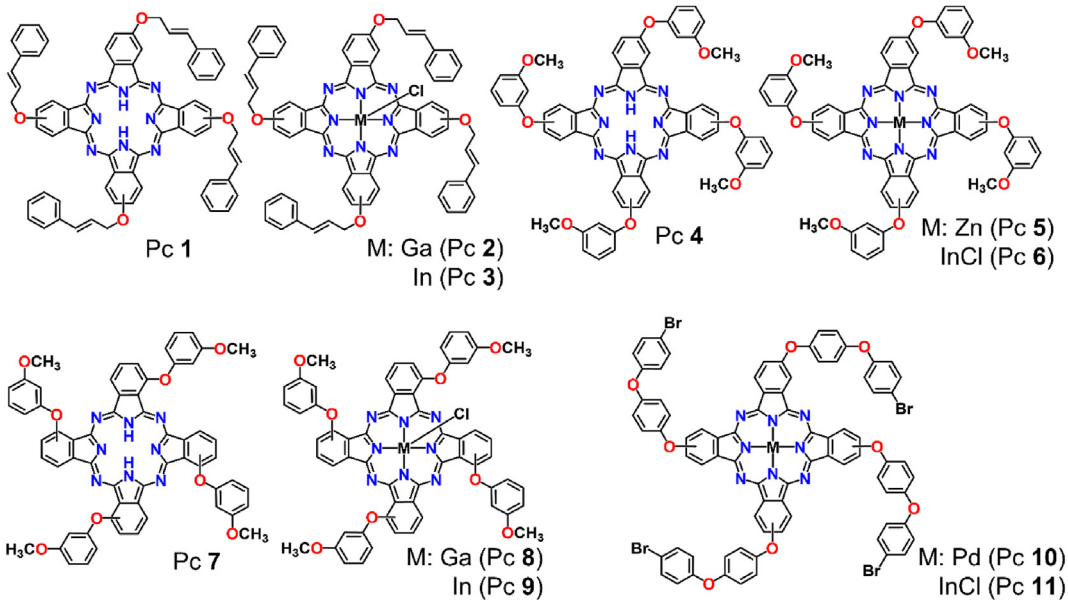

Figure 4 Structures of some of the reported Pcs used in the study of the effect of central in SDT/SPDT.

reported on the SPDT activity comparisons of Lu tetra-α- and β-substituted Pc **12** and Pc **13**, respectively. In this study, the $^1O_2$ yields were observed to be higher for the β-substituted Pc **13** compared to the α-substituted Pc **12** for both PDT and SPDT treatments. In the same study, the tetra-substituted Pcs were compared to the corresponding octa-β-substituted derivative, Pc **14**[65]. The SPDT $^1O_2$ yields were slightly decreased for the octa-substituted Pc **14** compared to the tetra-substituted Pc **13**. This effect is not yet clear. The sulfonated symmetrical AlS_4Pc (Pc **15**) and asymmetrical AlS_2Pc (Pc **16**) have been studied and have shown good SDT activities respectively[66–68]. Reduced symmetry of the Pcs structures is achieved by varying the number or type of R-groups on the Pcs structure[69]. For PDT, asymmetry in the Pcs structures has been reported to the increase the ROS yields are increased[70]. Low symmetry has also been reported to cause Q-band red-shifting when studied on a series of BODIPY-substituted ZnPcs[71]. Asymmetrical Pcs may also result in the destabilization of the HOMO resulting in the narrowing of the HOMO-LUMO gap and therefore the red-shifting of the Q-band. Although there is no current study comparing the symmetry of Pcs for SDT or SPDT, it would be interesting to explore the effect of symmetry by peripheral/non-peripheral R-groups variations on the sono-activities of Pcs.

4.2.2. *Effect of substituent-halogenation*

Halogens are highly electronegative atoms and will affect the electron-densities of Pcs when present in the Pcs' substituents. A halogenated Pc **17** bearing F and Cl atoms on peripheral R-groups has been reported and showed SDT activities[72]. Karanlık et al. compared the effects halogenation in SDT activities of tetra-β-substituted Pcs using F, Cl or Br on the R-groups[73]. The $^1O_2$ yields increased with increasing electron shells in the order Br > Cl > F. This observation was seen for the Pd Pcs (Pc **18**–Pc **20**)[73] and In Pcs (Pc **21**–Pc **23**)[74]. Atmaca et al. reported on the effect of halogenation on axially substituted SiPcs, Pc **24**–Pc **26**[75]. The ROS yields increased with increasing electron densities. For PDT, the effect of Pcs halogenation was reported for a fluorinated Pcs compared to its non-fluorinated counterpart[76]. Increased ROS yields were observed for the fluorinated Pcs. Furthermore, the redox-potential of the fluorinated Pc was higher and therefore more susceptible to electron transfer to O_2 or substrate for ROS generation through the type I and/or type II[76]. Halogenation may be beneficial for Pcs in SPDT.

4.2.3. *Effect of solubility and geometry*

The planar hydrocarbon structure of Pcs in addition to their conjugated core causes them to easily stack on each other through $\pi-\pi$ interactions[77,78]. This causes aggregation in aqueous media. The use of sp_3-hybridized and bulky substituents on the peripheral, non-peripheral, or axial positions on the Pcs structure has been reported to reduce aggregation[79–81]. Axial ligands alter the geometry of the Pcs and may improve their solubility[81,82]. A selection of various axially substituted SiPcs have been reported for SDT/SPDT, including the Pc **27**–Pc **40**[83–90]. Some of the Pcs with axial ligands that have been studied for SDT and or SPDT are shown in Fig. 6.

Molecular aggregation of Pcs is non-favourable since aggregation is known to promote photo-thermal conversion and reduced ISC[39]. In the case where photo-thermal therapy (PTT) is desired, this effect is ideal. However, for PDT, the ISC process is essential for ROS generation. Different moieties can be added to the axial positions of Pcs. This can be achieved when metal/metalloid centres with oxidation states of $\geq$3 such as In, Si or Sn etc. are used. Atmaca et al. reported on the SDT activities of Pcs with axial-ligands bearing quaternary N-groups with cations, Pc **37** and Pc **38**[89], and Pc **40**[90]. This further enhances the solubility of the Pcs compared to their neutral counterparts. Although Zhao reported on improved SDT activities of aggregated Pcs-artesenuate nanocomplex[91], this effect may not be beneficial when considering PDT since aggregation is known to reduce ISC. Moreover, the use of self-aggregated Pcs may not be ideal due to the requirement of increased drug concentrations for improved therapeutic efficacies.

Therefore, Pcs solubility is an important factor when designing Pcs for SPDT for cancer treatments. Another method for improving the solubility of Pcs include use of polar substituents such as $-SO_3^-$ [92,93], or $-CO_2^-$ [94], or $-OH$[95] and other ionic moieties[96,97].

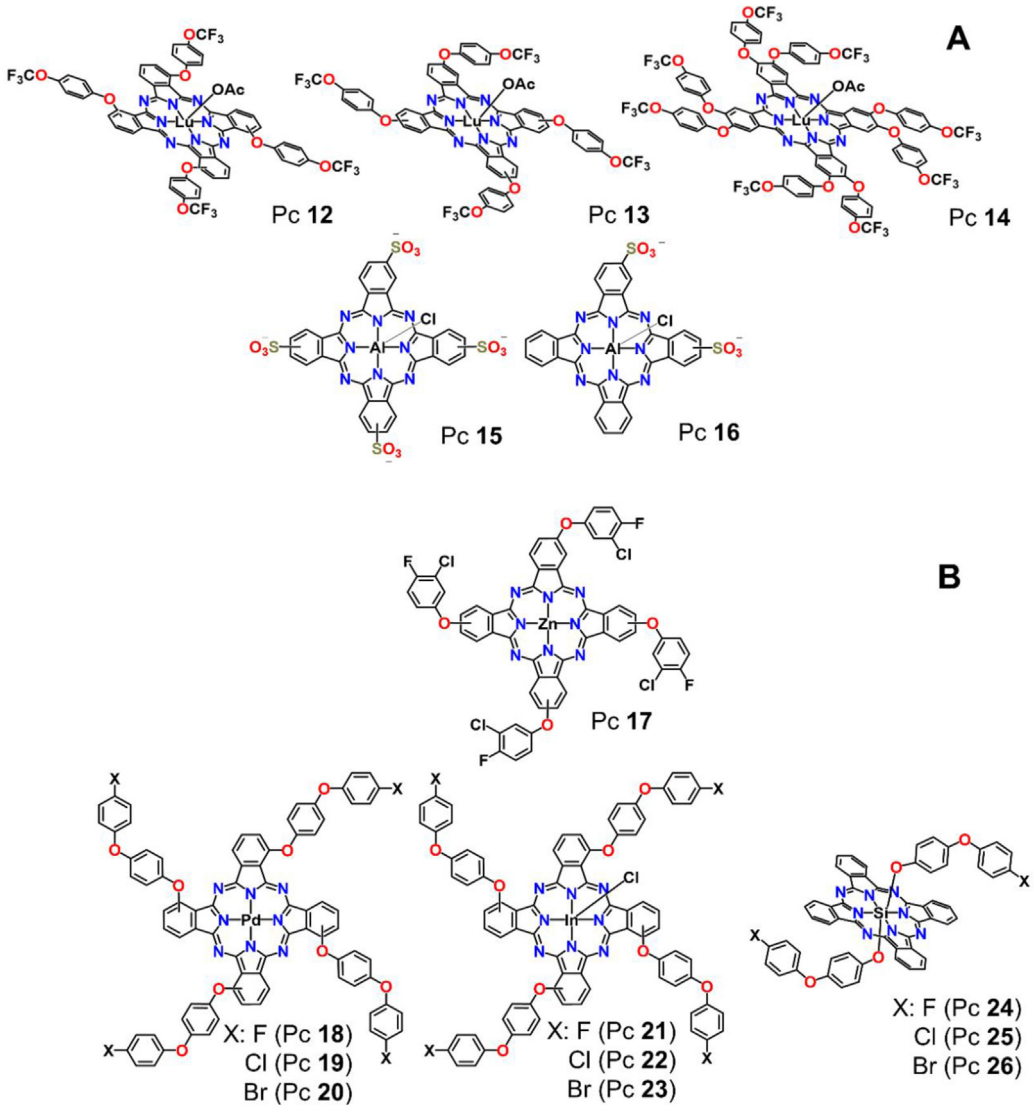

Figure 5 Structures of some of the Pcs used in the study of (A) the effect of point of R-group substitution, and (B) effect of R-group halogenation on the SDT and SPDT activities.

4.2.4. Effect of charge

The use of ionic substituents for Pcs is another common way of improving their solubility[98]. Charge fosters intermolecular electrostatic repulsion which results in reduced molecular stacking between Pc molecules. Some of the ionic Pcs that have been reported in SDT/SPDT are shown in Fig. 7.

The cellular membrane of most cancers is anionic. This is attributed to the exposure of anionic phospholipids on the surfaces of cancer membrane[99,100]. Moreover, the mitochondrial membrane potential is relatively higher[101,102], thus cationic cancer therapeutics are facilitated more easily into the mitochondria once they've accumulated within the targeted cancer cells[103]. The mitochondrion is famously known as the powerhouse of the cells and is crucial for various bio-energetic and bio-synthetic processes within the cells. The destruction of this organelle promotes antiproliferative and cell death pathways. Organelle-targeting allows for more precise therapy[104]. Cationic Pcs have gained much interest in the development of cancer therapeutics, as sensitizers in PDT and SDT. Pcs bearing R-groups with quaternary amines are a common way of introducing cations to the Pcs' structures. Various quaternizing agents have been used in the preparation of these as seen in Fig. 7. The Pc **41** and Pc **43** with tetra-cations on the morpholine moieties showed increased anticancer activities compared to the zwitterionic Pc **42** and Pc **44** counterparts[105]. The zwitterionic Pcs were prepared using propane-sultone which introduces anionic sulfonic-groups in addition to the cationic charge on the N-group. This enhanced efficiency of cationic Pcs may be attributed to the enhanced cellular uptake. The Pc **45**—Pc **48** have also shown impressive anticancer effects in SPDT[105]. For the Pc **47** and Pc **48**, the triphenylphosphine (TPP) moiety was used as a quaternizing agent for pyridine and morpholine ZnPc. The TPP enhances the sono-activities of the Pcs by ROS yields and anticancer efficiencies[105]. Furthermore, the TPP-moiety is known to target the mitochondria and may therefore improve anticancer activities through the organelle-destruction effect.

In addition to improved solubility and cancer cell targeting, ionic therapeutics including Pcs have shown selective binding to the albumin proteins[106]. Albumins proteins are the most abundant in blood and are generally targeted as transport proteins for various therapeutics. This group of proteins are also largely

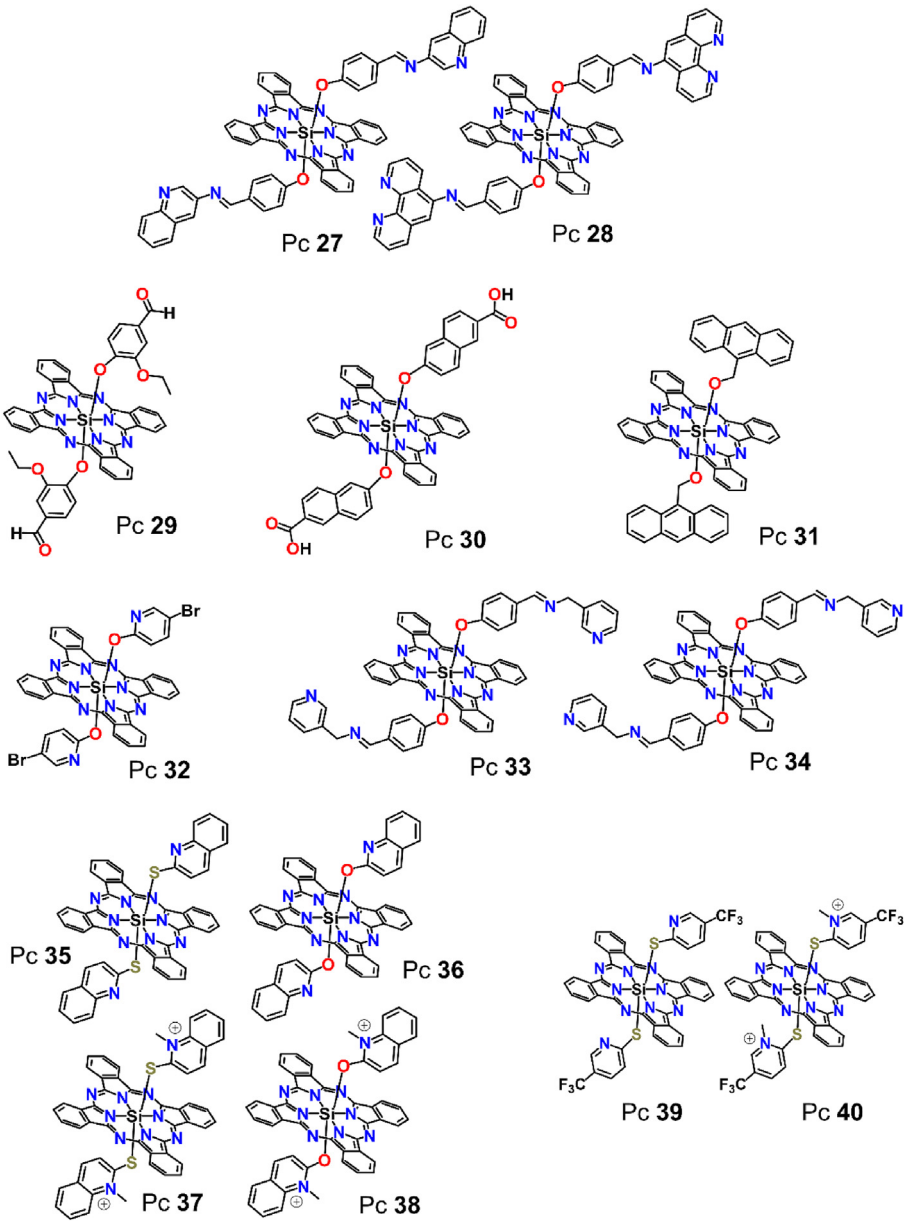

Figure 6 Structures of some of the axially substituted Pcs reported in SDT and SPDT studies.

involved in the regulatory transport of both endogenous and exogenous molecules. Therefore, ionic Pcs may be crucial in ensuring effective therapies in SPDT. A summary of Pcs reported for anticancer SPDT is given in Table 1.

A summary of the Pcs with varying structural designs is given in Table 2. Most of the Pcs used are metallic Pcs with substituents on the peripheral, non-peripheral or axial position. The operation parameters of the ultrasound used in the SDT studies for these Pcs vary (Table 2). While most of the studies focused on determining the photo and sono-chemical properties of the different Pcs, some continued with the evaluation of the anticancer activities *in vitro* and/or *in vivo*.

4.3. Pcs supramolecular structures for SDT and SPDT

Pcs can be modified through conjugation to other sensitizers to form Pcs-supramolecular structures for enhanced therapeutic efficacies. The structures of the reported Pcs-supramolecules in SDT are shown in Fig. 8.

Liu et al. reported on the design and SDT activities of tetra-4-carboxyphenoxy ZnPc (Pc **49**) and its polymer derivative Pc **50**[107], Fig. 8. The SDT and SPDT efficacies, as well as the intracellular uptake of the supramolecular Pc **50** was more enhanced compared to monomeric Pc **49**[107]. This observation was made in both the MCF-7 and Hep 1-6 cells *in vitro and in vivo*. The IC_{50} values (μmol/L) were also higher for the Pc **50** compared to the Pc **49** for both PDT and SDT activities. Pc−Ru-complex supramolecules have also been reported in SDT studies of Pcs. The peripherally Ru-complex labelled-ZnPc Pc **51** showed improved $^1O_2$ yields under SPDT treatments, with $^1O_2$ quantum yields of 0.72 compared to the PDT treatments, with $^1O_2$ quantum yields 0.66[108]. The axially Ru-complex-labelled SiPc Pc **52** showed almost twice the $^1O_2$ yields in SPDT compared to PDT treatments[109]. When comparing the Pc **51** to the Pc **52**, the peripherally substituted Pc performed

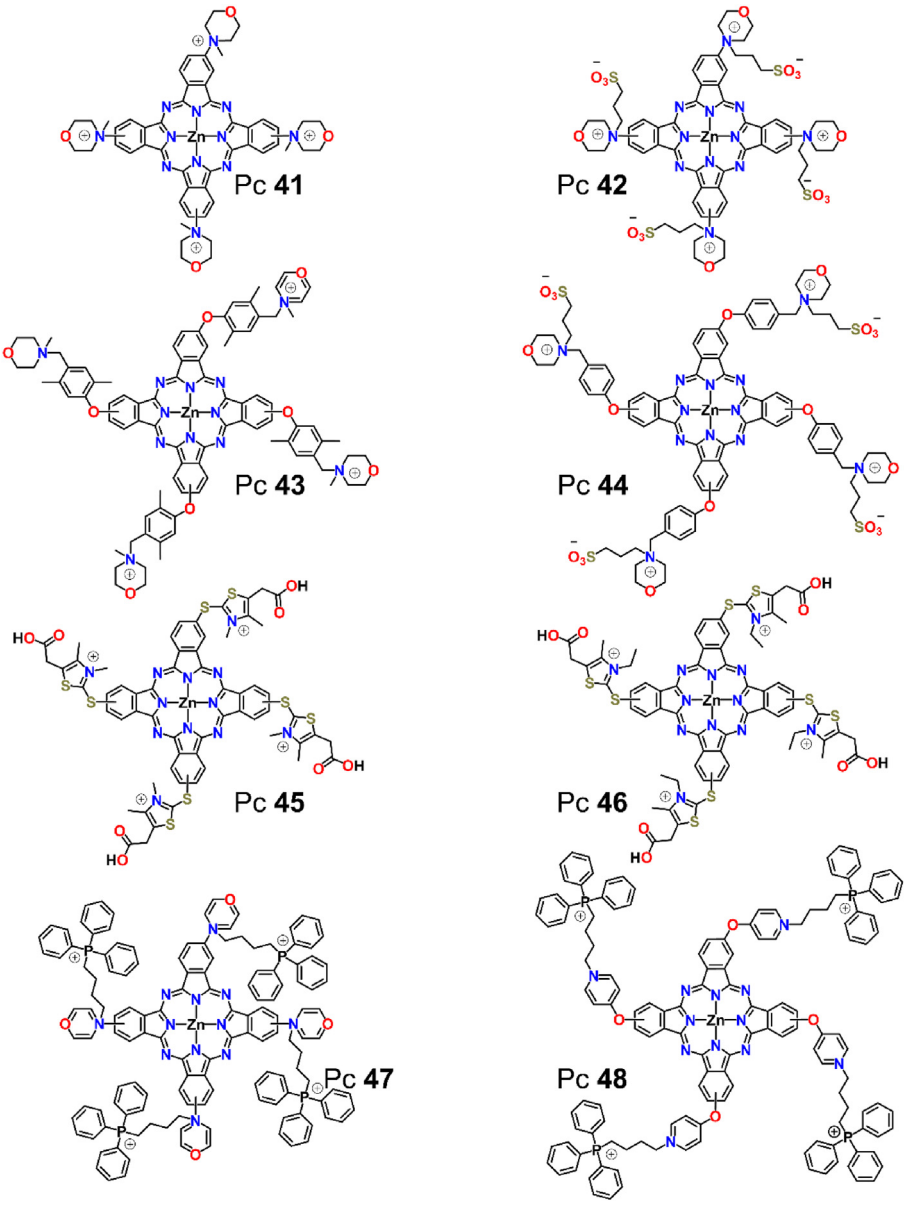

Figure 7 Structures of some of the Pcs bearing cationic substituents reported in SDT and SPDT studies.

better in terms of ROS yields compared to the axially ligated Pc **52**. Generally, Pc-supramolecular complexes are observed to demonstrate an increase in the SDT/SPDT efficiencies compared to the less bulky counterparts. This effect may be due to sensitizer-size increases, which may allow for increased surface area for bubble nucleation during acoustic-cavitation. Although this is the consideration, it was not necessarily the observation when comparing the tetra-substituted LuPcs (Pc **13**) to the bulkier octa-substituted LuPcs (Pc **14**)[65] which is also an example of increased molecular size. It is important to consider the possibility of exceptions. Moreover, it may be considered that supramolecules which constitute polymetallic subunits, >1 metal atom in the supramolecular frameworks (such as complexes between Pc−Pc or Pc-metallic moiety) have a greater chance of exhibiting enhanced SPDT. This may be influenced by the heavy atom effect in combination with enhanced acoustic cavitation. Finally, the use of more than one sono/photoactive molecules in constructing supramolecules may afford dual sensitization and therefore enhance SPDT effects.

5. Nanoparticle-Pcs systems for SPDT

Nanoparticles (NPs) have been extensively studied in the development of cancer therapeutics as they offer a variety of benefits. Pc−NPs complexes have been studied in PDT, SDT and SPDT and are reported in the literature. Some of the Pc−NPs-complexes comprise of liposomes[110], micelles[111,112], graphene oxide (GO)[72], graphene quantum dots (GQDs)[113], metallic NPs[114], protein complexes[115,116], and magnetic NPs[117]. The Pc−NPs complexes reported in sono-therapies for cancers are shown in Fig. 9. A summary of Pc−NPs complexes reported in SDT is given in Table 2.

Table 1 A summary of Pcs reported in SDT and SPDT studies.

Compd.	λ_{max} (nm)	Study	Parameters (US/light)	Cell line	Model	General observation	Ref.
Pc **1** Pc **2** Pc **3**	704[a] 708[a] 722[a]	SPDT	1 MHz, 0.5 mW/cm^2, 60 s 0.5 mW/cm^2, 60 s	Gastric (MKN-28) cells	*In vitro*	Increase in $^1O_2$ yields for SPDT compared to PDT treatments. The $^1O_2$ yields and cytotoxicity efficiencies were higher for the metallated Pcs compared to free-base (In > Ga > H_2).	57
Pc **4** Pc **5** Pc **6**	705 684 700	SPDT	35 kHz, 50 s 7.05 × 10^{15} photons/(s·cm^2), 50 s	–	–	Increase in $^1O_2$ yields and cytotoxicity for SPDT compared to PDT treatments. The $^1O_2$ yields were higher for the metallated Pcs compared to free-base (In > Zn > H_2).	58
Pc **7** Pc **8** Pc **9**	725[a] 720[a] 724[a]	SPDT	35 kHz, 320 W, 20 s 7.05 × 10^{15} photons/(s·cm^2), 20 s	–	–	Increase in $^1O_2$ yields for SPDT compared to PDT treatments. The $^1O_2$ yields were higher for the metallated Pcs compared to free-base (In > Ga > H_2).	59
Pc **10**	684	SPDT	35 kHz, 20 s	–	–	Increase in $^1O_2$ yields for SPDT compared to PDT treatments.	60
Pc **11**	699	SPDT	35 kHz, 10 s 7.05 × 10^{15} photons/(s·cm^2), 10 s	–	–		61
Pc **12** Pc **13** Pc **14**	690[a] 679[a] 679[a]	SPDT	35 kHz, 10 s 7.05 × 10^{15} photons/(s·cm^2), 10 s	–	–	Increase in $^1O_2$ yields for SPDT compared to PDT treatments. The β-substituted Pcs showed enhanced activity compared to the α-substituted. The tetra-substituted Pcs were better compared to the octa-substituted Pcs.	65
Pc **15**	682	SDT	1.93 MHz; 6.0 W/cm^2, 180 s	Human leukocyte (HL60) cells	*In vitro*	Apoptotic cells and caspase-3 activity observed during SDT treatments.	66
	682	SPDT	–	Prostate (PC3, LNCaP) cells	*In vitro*	Increase in ROS yields and anticancer activities for SPDT compared to PDT and SDT treatments. The methylene blue showed higher cytotoxicity compared to the Pcs.	67
Pc **16**	–	SDT	3 MHz, 1.0–3.0 W/cm^2, 60 s	Colon-26 cells	*In vitro* and *in vivo*	Bleomycin improve SDT cytotoxicity of the Pcs. An increase in caspase-3/7 observed for bleomycin-Pc-SDT.	68
Pc **18** Pc **19** Pc **20**	681 682 683	SPDT	35 kHz, 20 s 7.05 × 10^{15} photons/(s·cm^2), 20 s	–	–	Increase in $^1O_2$ yields for SPDT compared to PDT treatments. SPDT activities increased with increasing electronegativity (F > Cl > Br)	73
Pc **21** Pc **22** Pc **23**	710 710 712	SPDT	35 kHz, 20 s 7.05 × 10^{15} photons/(s·cm^2), 20 s	–	–	Increase in $^1O_2$ yields for SPDT compared to PDT treatments. SPDT activities increased with increasing electronegativity	74
Pc **24** Pc **25** Pc **26**	685 685 685	SPDT	35 kHz, 20 s 7.05 × 10^{15} photons/(s·cm^2), 20 s	–	–	(F > Cl > Br).	75
Pc **27** Pc **28**	684 674	SPDT	35 kHz, 10 s 7.05 × 10^{15} photons/(s·cm^2) 10 s	–	–	Increase in $^1O_2$ yields for SPDT compared to PDT/SDT treatments.	83
Pc **29**	687	SPDT	35 kHz, 20 s 7.05 × 10^{15} photons/(s·cm^2), 20 s	–	–		84

(*continued on next page*)

Table 1 (*continued*)

Compd.	λ_{max} (nm)	Study	Parameters (US/light)	Cell line	Model	General observation	Ref.
Pc **30**	683	SPDT	35 kHz, 20 s 7.05×10^{15} photons/(s·cm^2), 20 s	–	–	The $^1O_2$ yields of axially-substituted Pcs is enhanced compared to $SiCl_2$. The SPDT yields are higher compared to PDT treatments.	85
Pc **31**	674	SPDT	35 kHz, 20 s 7.05×10^{15} photons/(s·cm^2), 20 s	–	–	Increase in $^1O_2$ yields for SPDT compared to PDT treatments	86
Pc **32**	674	SPDT	35 kHz, 20 s 7.05×10^{15} photons/(s·cm^2), 20 s	–	–		87
Pc **33**	696	SPDT	35 kHz, 20 s 7.05×10^{15} photons/(s·cm^2), 20 s	–	–		88
Pc **34**	695						
Pc **35**	673	SPDT	0.5 W, 60 s 0.5 mW/cm^2, 60 s	Prostate (PC3) cells	*In vitro*	ROS yields of axially-substituted Pcs is enhanced compared to $SiCl_2$. Cytotoxicity increased for SPDT compared to PDT treatments. The quaternized Pcs showed enhanced cytotoxicity.	89
Pc **36**	673						
Pc **37**	680						
Pc **38**	676						
Pc **39**		SPDT	1.0 MHz, 0.5 W/cm^2, 60 s 0.5 mW/cm^2, 60 s	Prostate (PC3) cells	*In vitro*	Increase in cell death through apoptosis increases for SPDT compared to PDT and SDT monotherapies	90
Pc **40**							
Pc **41**	674	SPDT	1.0 MHz, 1.0 W/cm^2, 10 min 170 J/cm^2, 10 min	Cervical (HeLa) and breast (MCF-7) cell	*In vitro*	The $^1O_2$ and ·OH yields generally increases in SPDT compared to PDT and SDT alone. The cationic Pcs show better cytotoxicity compared to the zwitterionic Pcs.	105
Pc **42**	647						
Pc **43**	669						
Pc **44**	642						
Pc **47**	648	SPDT	1.0 MHz, 1.0 W/cm^2, 10 min 170 J/cm^2, 10 min	Cervical (HeLa) and breast (MCF-7) cell	*In vitro*	The $^1O_2$ and ·OH yields, and cytotoxicity generally increases in SPDT compared to PDT and SDT alone. TPP-labelled Pcs show impressive cell-internalization and association to BSA.	105
Pc **48**	633						

[a]Values in THF.

Table 2 Summary of Pc-supramolecules and NPs/protein conjugates reported in SDT or SPDT studies.

Compd.	λ_{max} (nm)	Adjuvant	Study	Parameters (US/light)	Cell line	Model	General observation	Ref.
Pc **17**	675 (THF)	GO	SPDT	35 kHz, 10 s 7.05×10^{15} photons/(s·cm^2), 10 s	–	–	Increase in $^1O_2$ yields for SPDT compared to PDT treatments for the ZnPcs and the conjugates. A slight decrease $^1O_2$ yields was observed for the conjugates.	72
Pc **41**	673	GQD	SPDT	1.0 MHz, 1.0 W/cm^2, 10 min 170 J/cm^2, 10 min	Breast (MCF-7) cell	*In vitro*	The $^1O_2$ and ·OH yields, and cytotoxicity generally increases in SPDT compared to PDT and SDT.	113
Pc **45** Pc **46**	685 684	AuNPs AgNPs	SPDT	1.0 MHz, 1.0 W/cm^2, 10 min 170 J/cm^2, 10 min	Cervical (HeLa) and breast (MCF-7) cell	*In vitro*	The $^1O_2$ and ·OH yields, and cytotoxicity generally increases in SPDT compared to PDT and SDT alone. The conjugates generally performed better.	114
Pc **49** Pc **50**	675 675	Pc-polymer	SDT PDT	1.0 MHz, 3.0 W/cm^2, 5 min 280 mW/cm^2, 15 min	Breast (MCF-7) and mouse hepatoma (Hep 1-6 and H22) cells	*In vitro* and *in vivo*	The $^1O_2$ yields and cytotoxicity efficacies increased for polymer Pc compared to the monomeric Pc. The polymer Pc showed enhanced cellular uptake.	107
Pc **51**	680	Ru-complex	SPDT	35 kHz, 20 s 7.05×10^{15} photons/(s·cm^2), 20 s	–	–	Increase in $^1O_2$ yields for SPDT compared to PDT. The PDT $^1O_2$ yields were lower compared to ZnPc.	108
Pc **52**	674	Ru-complex	SPDT	35 kHz, 20 s 7.05×10^{15} photons/(s·cm^2), 20 s	–	–	Increase in $^1O_2$ yields for SPDT compared to PDT.	109
Pc **53**	670	ZnPc Liposome	SPDT	1.1 MHz, 1.0 W/cm^2, 10 min 300 J/cm^2, 10 min	Colon carcinoma (CT26)	*In vivo*	Tumour diameter reduces for SPDT treatments compared to PDT and SDT.	110
	–	DSPE-PEG Micelles	SDT	20 kHz, 10 W/cm^2, 5 min	Melanoma (B16F10) cells	*In vitro*	Micelles showed enhancement of ROS yields and cytotoxicity efficacies of Pcs in SDT.	111
Pc **54**	–	DSPE-PEG Micelle	SDT	30 kHz, 10 min	HUVECs and breast (4T1) cells	*In vitro*	Increased $^1O_2$ and ·OH yields and tumour volume reduction for the nanocomposite compared to the Pcs alone during SDT.	112
Pc **55**	688	BSA protein	SDT	1.0 MHz, 2.0 W/cm^2, 3 min	Hepatoma (HepG2) cells	*In vitro* and *in vivo*	The BSA improved the $^1O_2$ yields and SDT efficacy of the Pc. The tumour volumes *in vivo* were greatly decreased for cells treated with oxygenates nano-complex.	115
Pc **56**	636	HAS and Hb protein	SDT	1.0 W/cm^2, 2 min	Breast (4T1) cells	*In vitro* and *in vivo*	The oxygenation of Hb improves the O_2-availability in the cells and therefore enhances SDT efficiencies and cytotoxicity. The $^1O_2$ yields were evident for the SDT treatments in the presence of the nano-complexes.	116
Pc **57**	682	FeS_2-PEI	SDT	1.0 MHz, 1.0 W/cm^2, 5 min	Hepatoma (HepG2) cells	*In vitro* and *in vivo*	The FeS_2 increased the ROS yields and cytotoxicity efficiency of the Pcs under sono-treatments. The tumour volumes *in vivo* were greatly decreased.	117

5.1. *Enhanced cellular specificity, uptake and pharmacodynamics*

Generally, NPs are used as delivery vectors for therapeutics, including Pcs, to cancer sites[118,119]. Cancer cells have a leaky vasculature, where nutrients are easily internalized[120,121]. The use of NPs (1100 nm) allows for the passive uptake of sensitizers by cells through a phenomenon known as enhanced permeation retention[122–124].

The design of Pc-NPs conjugates may be achieved through different kinds of interactions as shown in Fig. 9.

Pcs may be designed with specific functional groups to facilitate their conjugation to the NPs surfaces through various synthetic routes. For example, covalent amide bonds may be formed by reacting −COOH on Pcs and $-NH_2$ groups on NPs and *vice versa*, or R-groups bearing −N or −S atoms may be used to allow for spontaneous affinity bonds to metallic NPs (including Ag and Au)[70,114]. Alternatively, non-covalent interactions including $\pi-\pi$ stacking between carbon GQDs and Pcs, or association of lipophilic Pcs to lipophilic lipid tails allows for relatively facile encapsulation of Pcs in lipid NPs. Pcs are also known to non-specifically bind to BSA proteins and will therefor interact with the protein to form nano-complexes[95,106]. The Pcs−NPs complexes are designed with careful consideration for specific targeting and accumulation of the sensitizer at the tumour site. Additionally, NPs have been employed in improving the delivery of lipophilic drug molecules through aqueous biosystems, therefore addressing the limitation of non-soluble drug molecules and improving their biodistribution. For *in vivo* studies, Pcs generally conjugated to NPs showed enhanced tumour targeting compared to their non-conjugated counterparts[110,117]. Bakhshizadeh et al. uses liposomes to encapsulate the hydrophobic ZnPc forming liposomal ZnPc nano-complexes, Fig. 9 [110]. These nanocomplexes have improved biodistribution and are able to accumulate at the tumour sites in the BALB/c mice, reducing the tumour volumes after SDT treatments[110]. Yin et al. also reports on the efficient

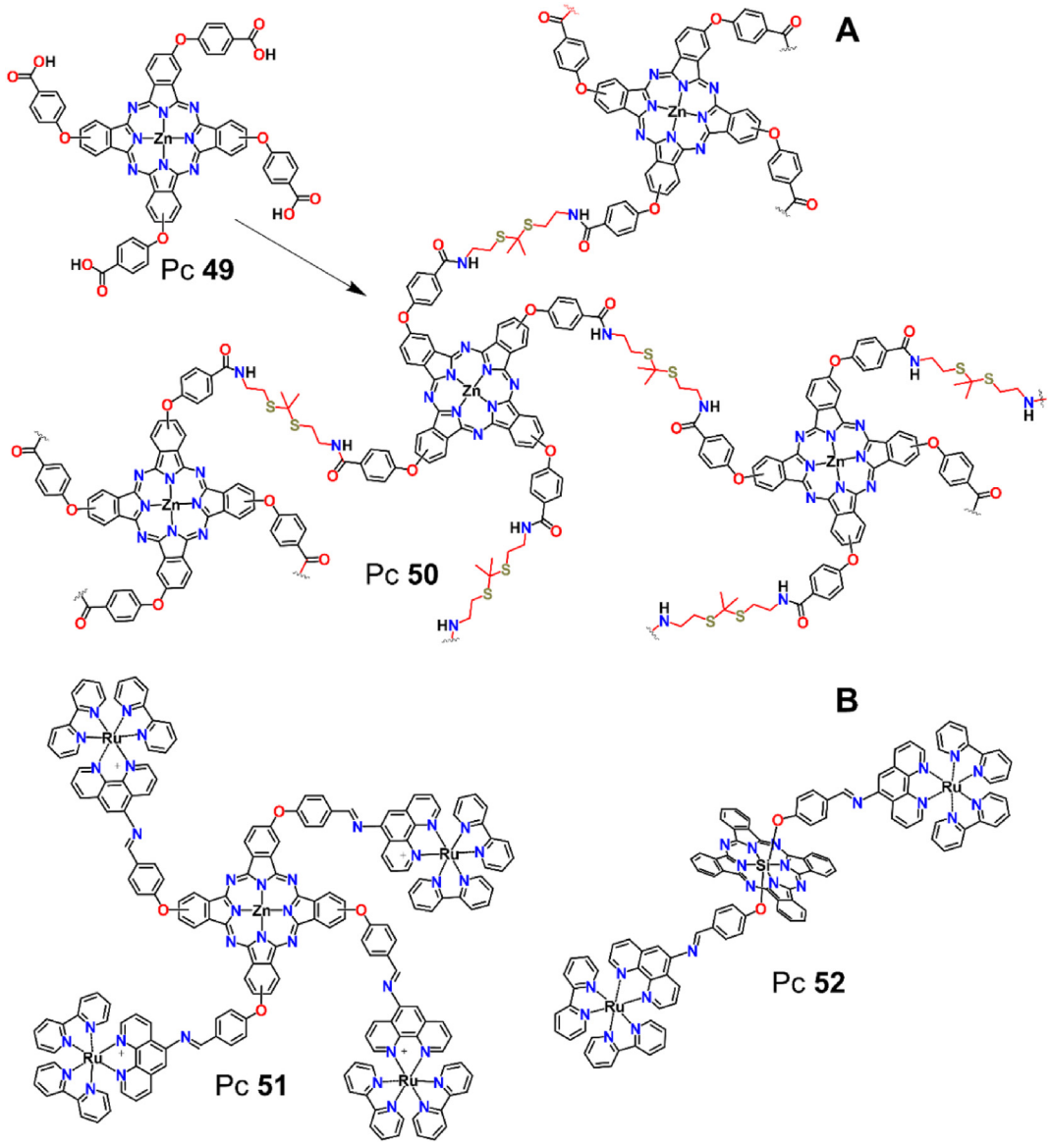

Figure 8 Structures (A) Pc-based polymer and (B) Ru-complex-labelled Pcs supramolecules.

tumour targeting and accumulation of the HAS-Hb Mn-tetra-sulfonate Pc **56** conjugated to HAS-Hb (complex as shown in Fig. 9) in mice models bearing the 4T1 breast cancer[116]. The MRI images show increased cellular content of these nano-complexes over 3 h[116]. The Pc **56** are intercalated within the nano-complex with the HAS and Hb proteins, and may also be bound to the hydrophobic pockets of the HAS proteins. The intracellular release of the Pcs in the nano-complex have been shown to be triggered by the overexpressed intracellular glutathione in the cancer cells[116]. Li et al. reported on the design specific tumour targeting of the Pc **57** when conjugated to FeS_2-PEI[117]. This study reports on the reaction of the nano-complexes with intracellular H^+ atoms to induce the release of the Pc **57**[117]. The SDT intracellular ROS yields and cell death percentages were increased for cells treated with the Pc **57**−FeS_2 complexes compared to those treated with the non-conjugated Pc **57**[117]. For the *in vivo* studies, the accumulation of the nano-complexes at the tumour sites were shown to be higher relative to the accumulation of the Pcs alone. Additionally, the tumour volumes observed post SDT treatments were significantly decreased for mice models treated with the nano-complexes compared to those treated with the Pcs alone[117]. Overall, for efficient therapeutic efficacies for *in vivo* models, Pc-nano-complexes may be generally better suited, compared to Pcs alone. Nanoparticles generally improve the delivery and pharmacodynamics of the Pcs for SDT and SPDT as seen with increase tumour accumulation and anticancer efficiencies.

There are various synthetic routes that may be used for the preparation of Pc−NPs complexes. These are generally dependent on the physicochemical properties of the Pcs and NPs or NPs subunits. For example, similarity in polarity indices, opposite charges or $\pi-\pi$ conjugate systems, are examples of properties that may be used in the formation of Pc−NPs complexes through non-covalent interactions[72,113–116]. Otherwise, covalent interactions may be formed between the R-groups on Pcs to functional groups on the surfaces of the NPs[114]. Examples of the methods used in the preparation of Pc-NPs conjugates are shown in Fig. 10.

The Pc−NPs reported for SDT or PSDT have been prepared using different modification methods. Covalent amide bonds or non-covalent S-atom affinity bond to metallic Ag and Au NPs[114] as shown in Fig. 10. Non-covalent bonding of Pcs to Ps have been achieved by use of $\pi-\pi$ interactions on the flat surfaces of GQDs sheets and Pcs to achieve molecular stacking nano-complexation[113] or the spontaneous non-specific binding of Pcs to BSA proteins[115], Fig. 10, where cationic Pcs have been reported to demonstrate improved BSA binding behaviours[106]. Pcs are carbon-rich structure and are generally lipophilic. In the presence of lipids in a polar (aqueous) environment, Pcs may also form nanocomplexes with the lipids to form micelles, where a lipophilic core (comprising of the lipid lipophilic head) may be form and accommodate the Pcs molecules, Fig. 10. Liposomes are also formed similarly, where the lipid tails are bound together on the outer and inner shell, forming a lipid bilayer with a hydrophilic core. While some Pcs may also be encapsulated in the core, some will generally tend to associate with the lipophilic lipid tails and be intercalated within the bilayer (Fig. 10).

5.2. *NPs-assisted ROS yield enhancement*

NPs have been reported to play a major role in SPDT and are known to enhance acoustic cavitation by increasing the surface area for bubble nucleation and therefore enhancing ROS yields[125,126,127]. Various Pcs-NPs conjugates have been designed and studied for SDT and SPDT to a lesser extent compared to PDT for cancer therapy (Table 2). Some of the NPs studied in PDT have been reported in SDT alone and as adjuvants for Pcs. Graphitic nanoparticles such as graphene oxide (GO), or graphene quantum dots (GQDs) have been reported to act as donor and promote the transfer of energy to Pcs acceptors through Forster energy resonance transfer (FRET) during PDT[128,129]. FRET therefore allows for enhance ROS yields under light exposure. Although this is the case, a decrease in the ROS yields for both PDT and SPDT was observed when comparing ZnPc-GO conjugates compared to the ZnPc alone. There was no clear correlation in the *w*% of the GOs on the ROS yields of the conjugates[72]. It would be interesting to determine the ROS generation of the GOs alone. GQDs have been reported for SDT and SPDT where an enhancement in the ROS yields were observed for Pc **41** when conjugated to the GQDs[113]. GQDs alone have also shown ROS yields under ultrasound irradiations at 1.0 MHz, 1.0 W/cm^2 [113]. Considering the possible FRET effect under PDT and enhanced ROS generation in both PDT and SDT, the conjugation of Pcs to GQDs may be a benefiting strategy in the design of Pc-based sensitizers for SPDT. Metallic NPs are also known to improve ROS yields of Pcs through the heavy atom effect in PDT[130,131]. In SDT, the metallic AuNPs and AgNPs show an enhancement in the ROS yields of cationic thiazole Pc **45** and Pc **46**[114]. Moreover, the anticancer efficacies on MCF-7 and HeLa cells were generally increased in the presence of the NPs under the SPDT treatment. Various other NPs including mesoporous SiO_2 NPs[132], TiO_2 NPs[133,134] and graphene nanotubes[135] have been reported to enhance acoustic cavitation. These have however not yet been reported in combination with Pcs in SPDT of cancers.

5.3. *NPs-assisted hypoxia evasion*

Pc-based nano-complexes have also been reported as probes for sono-treatments in hypoxic cancers. SDT is known to initiate cytotoxic effects through both oxygen-dependant and independent routes (Fig. 3). The efficiency of SPDT may be greatly impacted in the absence of O_2. Yin et al. reported on the design of an O_2 self-supplementing nano-complex using Mn tetra-sulfonate Pc (Pc **56**), hemoglobin (Hb) and human serum albumin (HSA) to alleviate hypoxia in the treatment of 4T1 cells[116]. The NPs system with oxygenated Hb (HbO_2) was compared to the unoxygenated complex Hb to measure the effect on SDT. The HbO_2 allowed for an increase in the cellular accumulation of O_2 in hypoxic tumours resulting in increased anticancer SDT efficacies compared to the non-oxygenated Hb[116]. The HAS protein in this complex was mainly for tumour delivery purposes. Additionally, tumour tissues are known to have excess H_2O_2 compared to normal tissue and can therefore be a beneficial target for chemo-dynamic therapy (CDT). Li et al.[117] reported on the chemo-dynamic effect of FeS_2-polyethylene imine (FeS_2-PEI) and axially substituted SiPc (Pc **57**) nano-complex (FeS_2-Pc) in combination with SDT against HepG2. The FeS_2 formulates a programmable nano-complex which may be turned on and off by the regulation of intracellular H^+ and H_2O_2 to yield $\cdot OH$[117]. The generation of ROS through the CDT redox reactions allows for intracellular oxidative stress induction in hypoxic conditions. Enhanced ROS yields for the sono-treated FeS_2-Pc conjugate were observed compared to the sono-treated Pc **57** alone[117]. Moreover, the cell viability studies for the sono-treated cells showed high cytotoxicity for the CDT and SDT treated cells using the FeS_2-Pc nano-complex both *in vitro* and *in vivo*. The FeS_2 is also used as a bio-imaging probe

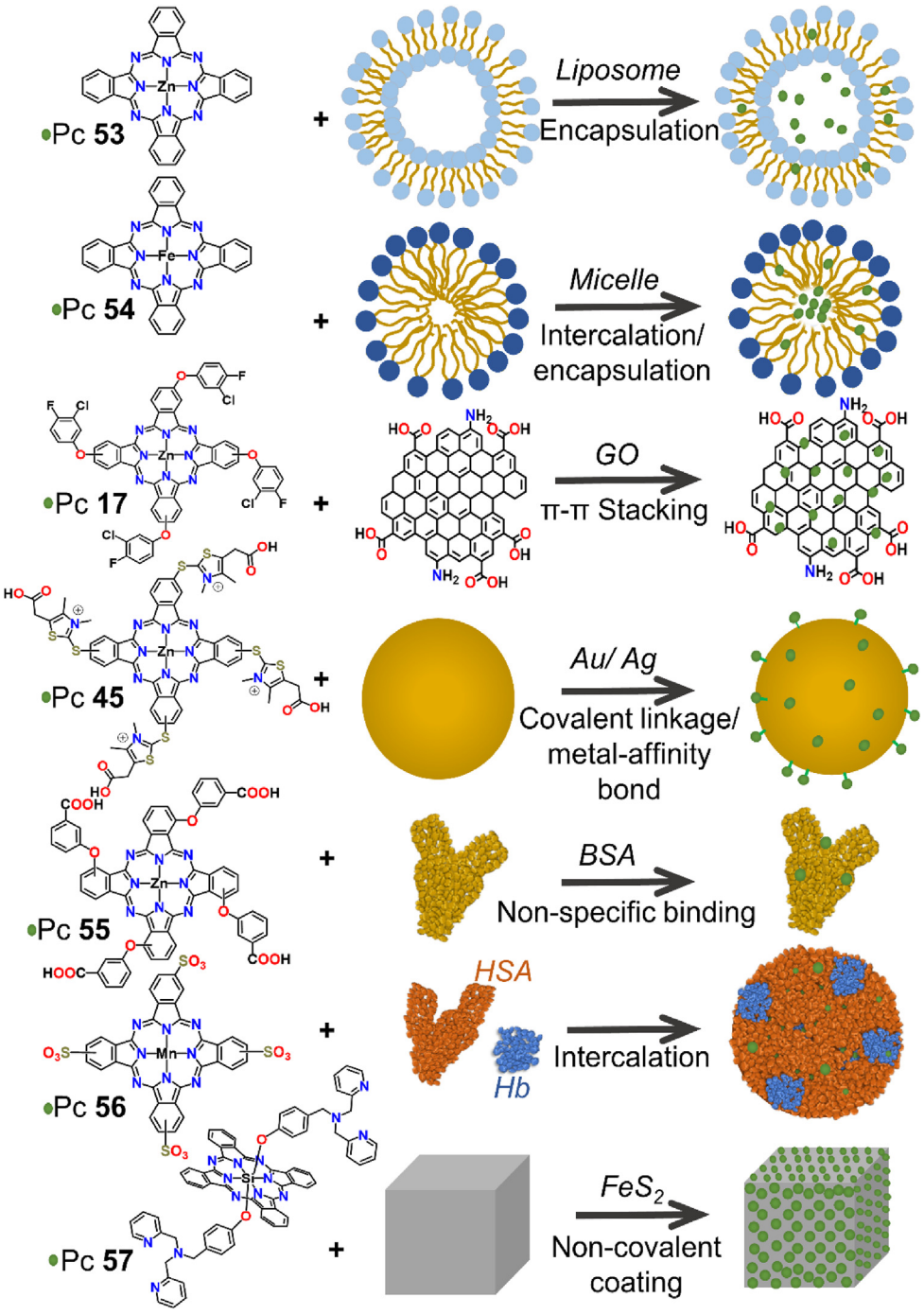

Figure 9 Structures of some of the Pcs and Pc−NPs conjugates reported in the effects of nano-complexes on the SDT and SPDT efficacies of Pcs. The formation of the nano-complexes is achievable through intercalation; encapsulation; stacking; or formation of covalent or non-covalent affinity bonding of the Pcs molecules to various adjuvants.

for magnetic resonance imaging of tumours *in vivo*[117]. The combination of imaging and therapeutic agents to form theranostic agents is crucial in the development of anticancer modalities as it allows for personalized and more precise therapy[136,137]. The FePc (Pc **54**) micelle nanodots are also reported to enhance the SDT effects through promoting CDT[112]. Although the study of CDT in combination with SPDT using Pcs-NPs conjugates has not yet been reported, it may be interesting to evaluate the therapeutic efficacies.

5.4. *Biocompatibility and toxicity considerations*

The design and application of Pcs and Pc−NPs complexes with minimal toxicity is essential for the SPDT of cancers for maintaining a non-invasive and controllable therapeutic approach. Pcs are generally reported to demonstrate none to minimal dark toxicity. Therefore, the use of Pcs as sensitizers for SPDT may allow for a controllable therapy. For PDT, the photodegradation quantum yields (Φ_d) for Pcs quantifies the rate of Pcs degradation

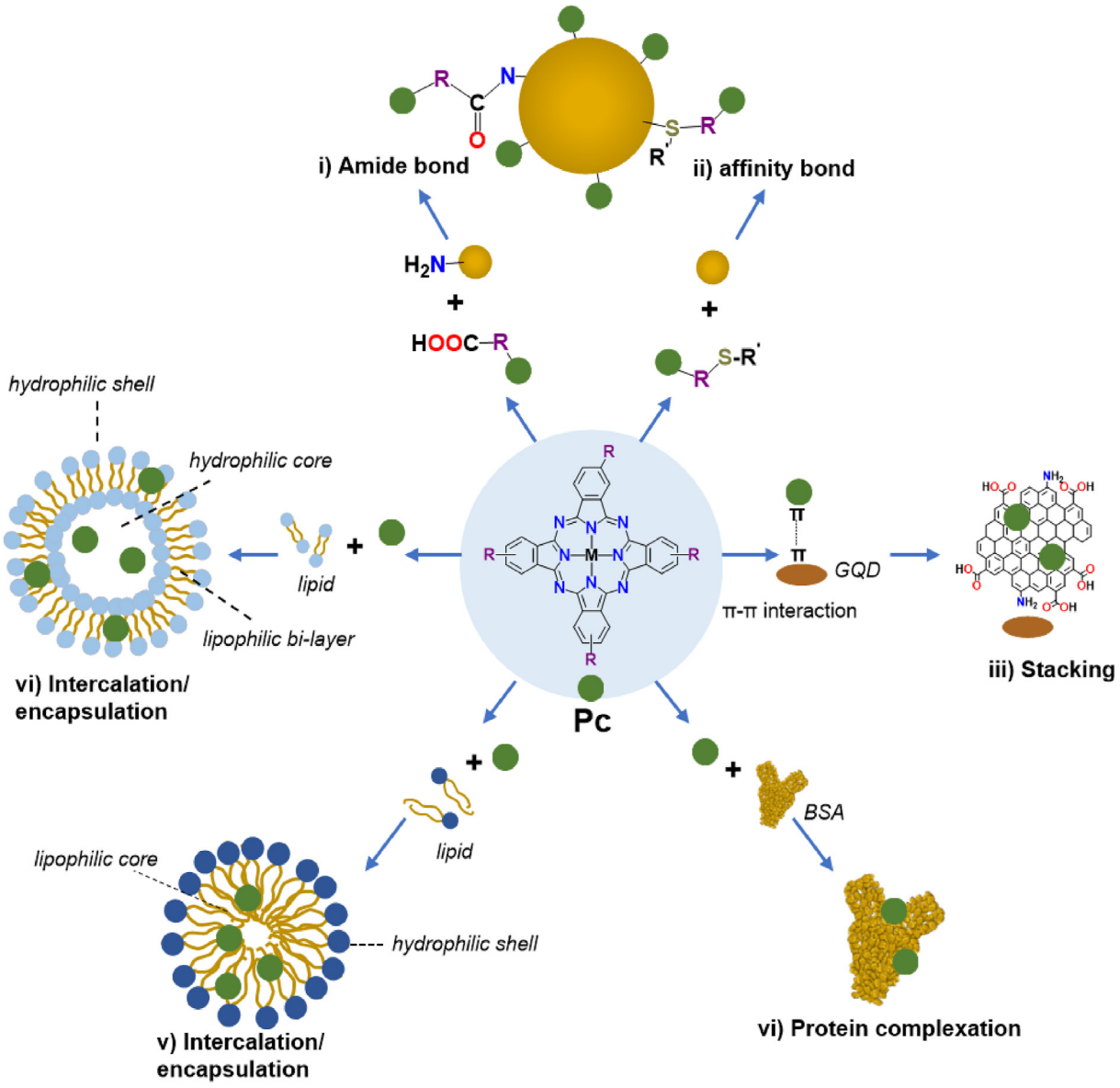

Figure 10 Examples of methods used for the preparation of Pcs-nanocomplexes.

upon exposure to light during PDT treatments. Güzel et al.[53], Karanlik et al.[58] and Atmaca et al.[60] reported on the calculation of the Φ_d values of different Pcs under light treatments monitored by UV−Vis spectroscopy, where the Φ_d values were in the 10^{-4} order. The low Φ_d values suggest relative stability of the Pcs under PDT conditions. For SDT, a function defining the stability of Pcs under US treatments has not yet been defined. However, the presence of carbon radicals (·C) under US treatments at higher frequency and power (2.0 MHz, 3.0 W/cm^2) were detected for ionic Pcs in another study suggesting possible fragmentation of Pc structures[105]. While this was the observation in this study, reducing the frequency and power to 1.0 MHz, 1.0 W/cm^2 showed reduced degradation and efficient SDT activities. Since the toxicity profiles of fragments that may be derived from degrading Pcs under light and/or US treatments, the stability of Pcs is important in order to minimize possible toxicity from the treatments[105]. The stability of NPs for therapy is equally important. Metallic NPs such a AgNPs are known to exhibit chemotoxicity by releasing metal ions as a result of ionization[138]. To minimize this effect, metallic NPs may be stabilized specific capping agents including: chemical moieties such as CTAB[139], GSH[140], polyethylene glycol (PEG)[141]; or biomolecules such as BSA[142], chitosan[143]. The capping agents, in addition to stabilizing NPs, may also serve as linkers for Pcs-conjugation to the NPs, as surfactants to improve solubility or biomarkers for cancer specificity and delivery[139,142]. Alternatively, a selection of biocompatible NPs have been reported and applied in PDT and SDT studies including liposomes, micelles, GQDs and SiO_2. Pcs complexed with these NPs have also been reported to show none or minimal dark toxicity[110,111,113,144] and may be a relatively favourable consideration for the development of Pcs-based therapeutics.

6. Experimental configurations

While altering the structures of the Pcs may lead to improving their SDT and SPDT performances, the ultrasonic operational parameters such as the frequency and power of the ultrasound are key considerations for Pc-mediated SDT and/or SPDT.

Furthermore, the order of light and ultrasound irradiation in SPDT is also key as it may affect the overall ROS yields and therapeutic efficiencies of the Pcs.

6.1. *Effect of ultrasonic parameters*

The frequency and power affect the physical properties of the ultrasonic mechanical waves exerted in the aqueous media, and in turn the cavitation efficiency during SDT[145,146]. An increase in the ultrasonic frequency results in rapid formation and implosion of the micro-bubbles[146–148]. Where an increase in the ultrasonic power increases the average radii of the forming bubbles[148]. Hypothetically, it may be expected that increasing both the frequency and power of the ultrasound may enhance the acoustic cavitation and ROS yields. While this might possibly be the case, the temperature and pressure changes are also increased where the stability of the Pcs may be compromised. The SDT activities of differently substituted-cationic Pcs has been reported under different ultrasonic parameters varying the frequency (1.0 and 3.0 MHz) and the power (1.0 and 2 W/cm^2)[105]. Generally, the ROS yields and cytotoxicity efficacies were more efficient at 1.0 MHz and 1.0 W/cm^2 for most of the Pcs. Increasing the frequency to 2 MHz and/or the power to 3.0 W/cm^2 generally resulted in reduced efficacies. Interestingly, in addition to detected ROS of the studied Pcs, ·C were also detected for some of the Pcs[105]. High energy under SDT may lead to localized increase in temperature and pressure which may in turn cause nearby carbon-based sensitizers, including Pcs, to fragment. Fragmentation may lead to the yield of sensitizer-derived ·C[149]. Fragmentation of Pcs under ultrasound exposure to yield ·C may also cause them to lose their electronic properties and SDT/SPDT activities and therefore greatly impact their overall efficacies. Moreover, ·C are also a threat to cancer cells since they may form peroxyls and alkoxyls upon reaction with O_2[150]. Considering this effect, the order of light and ultrasound irradiation in SPDT is important and should be considered for Pcs during treatments.

6.2. *Effect of order of irradiation*

The order of irradiation in SPDT has been shown to affect the therapeutic efficacies of Pcs[110]. While this effect is not clearly understood, Bakhshizadeh et al. reported on the reduced efficacies on cancers treated with the ultrasound first and light after when using Pcs[110]. In cases where the ultrasonic parameters cause the Pcs to fragment, irradiating ultrasound first may lead to loss of photosensitizing ability of the Pcs and reduced activity when light is administered. There have been no extensive studies reported on the stability and structures of Pcs under the simultaneous irradiation of light and ultrasound.

7. Conclusions and perspectives

Various strategies involving the structural modifications of Pcs may be applied to tailor their overall behaviours as agents for SDT and SPDT. While a wide range of Pcs structures have been designed and studied for SDT and SPDT, more details on the influence of some structural variations on the activity-profiles of the Pcs may still be explored and defined for these treatment modalities to greater extents.

The central metal plays an important role in light and/or ultrasound mediated cancer therapies. In addition to the NIR-shifting of the Q-bands, the T_1 is enhanced leading to increases ROS yields for metallated Pcs compared to the free-base counterparts. Since the mechanism of action in SDT involves sonoluminescence for ROS generation, the relationship of the Pcs' Q-bands to their SDT activities may be defined further to determine Q-band wavelengths that may allow for more effective sonoluminescence light absorption under different parameters. Generally, Pcs with metalloids; transition and post-transition metal-centers have been reported with impressive SDT and SPDT activities. Ln are known to result in extended coordination of two or more Pcs cores yielding double, triple, quadruple etc. decker supramolecular frameworks. The SDT activities of these type of complexes may be interesting to explore and study the effects of the type of Ln and number of layers of Pcs on the decker complexes. Additionally, the Pcs symmetry may be further studied for SDT. Pcs symmetries may be altered by adding different R-group types on the peripheral and non-peripheral positions. A comparative study looking at the effect of reduced symmetry in comparison to symmetrical Pcs would be beneficial in further determining strategies for enhancing their therapeutic efficacies in sono-therapies.

NPs and biologically active adjuvants are undoubtedly advantageous for Pcs in SDT. Researchers have shown improved solubility; tumour targeting and delivery; drug internalization, as well as improved ROS and cytotoxicity efficiencies in Pcs-NPs conjugates. With regards to ROS yields, NPs are reported to promote ISC of the photo-activated excited Pcs into the T_1 and consequently enhance ROS yields. NPs alone have also demonstrated ability to generate ROS under sono-treatments, where the combination of NPs with Pcs may afford a dual-sensitizer complex for SDT with enhanced ROS yields. Another important benefit to NPs in Pcs-mediated SDT and SPDT is the ability of some NPs to relieve hypoxia by generating ROS through the Fenton reaction, a CDT effect. PDT is known to largely depend on the availability of O_2 to allow for effective cancer eradication. While SDT also depends on O_2 for therapy, it is also reported to promote other non-O_2-dependant processes. However, the design of hypoxia-minimizing nano-complexes and Pc−NPs CDT agents may be beneficial in addressing the issue of hypoxia for effective SPDT in cancer therapy. SDT may possibly lead to hyperthermia, and some NPs may promote this effect. Designing Pcs for PTT by tailoring their molecular structures may cause a suppression in their PDT activities since the occurrence of photo-thermal conversion (important for PTT) results in reduced ISC (important for PDT). The use of heterogenous Pc−NPs complexes where the Pcs are involved in the PDT and SDT, and the NPs in CDT, may be ideal. In this case, the structural pre-requisites of Pcs for SPDT may be appreciated. Studies focusing on the PTT effect of SDT using Pcs may be beneficial in further defining the mechanisms of Pcs-mediated SDT and additional factors affecting these mechanisms thereof. In addition to NPs and proteins, there are various other adjuvants that may be applied to enhance the efficacies of Pcs in SDT and SPDT. For PDT, plant-derived complexes (phytochemicals) have been studied and shown to enhance efficacies[151–153]. The study of phytochemicals in combination with Pcs for SDT and SPDT may be interesting to explore.

Some of the *in vitro* and *in vivo* SDT studies reported in the literature have shown how the treatments affect cellular biochemistry. The activation of caspase reactions and DNA destruction have been reported for Pcs-mediated SDT to explain the effect of cytotoxicity. There is, however, a gap in the definition of intracellular mechanisms that are triggered during SDT including protein or hormone up- and down-regulations which ultimately lead to cell death. Studies which may define molecular

process involved in SDT in general (including Pcs-mediated SDT), are crucial in fully defining the mechanism of action involved in SDT for cancer therapy. Moreover, a closer look on the influence of the Pcs' structures (along with other sensitizers), on the SDT-initiated cellular biochemical responses, is paramount in understanding this treatment modality.

The ultrasonic parameters do affect the overall Pcs' behaviours under ultrasound exposure. The parameters are reported to affect the cavitation efficiencies, thus affecting the properties of the sonoluminescence emission as well as the bubble size and formation rates. This generally affects the amount of ROS yields. Additionally, the temperature and pressure within the microenvironment will be affected. Pcs may fracture under specific ultrasonic conditions during SDT. It is therefore important to determine the optimum conditions for Pcs used in SDT. For SPDT treatments where the ultrasound and light are administered sequentially, the effect of the order of irradiation also needs to be determined prior the application of the treatment modality. While studies have shown the reduced activities of Pcs when the ultrasound is administered first and light after, this effect is not yet clearly defined. For some Pcs, the formation of ·C was evident indicating the formation of Pc-derived fragments. Studies focusing on the isolation and characterization of Pcs' structures before and after ultrasound irradiations may be beneficial in determining the effects of the ultrasound on the Pcs structures and potentially define the principle behind the order of irradiation in SPDT.

Overall, Pcs are impressive sensitizers for SPDT. Their structural versatilities afford them the great interest in the development of improved anticancer modalities for the treatment of a wide range of cancer types.

Acknowledgments

This study was supported by the National Research Foundation of South Africa. This work is based on the research supported by the South African Research Chairs Initiative of the Department of Science and Technology and National Research Foundation of South Africa (Grant No. 98337). The authors sincerely thank the University of Johannesburg, the National Laser Centre, and the National Research Foundation−South African Research Chairs Initiative (NRF-SARChI) for their financial grant support.

Author contributions

Lindokuhle Cindy Nene: conceptualization, writing-original draft preparation, illustration of figure; Heidi Abrahamse: Writing, review and editing, supervision, funding acquisition, administration.

Conflicts of interest

This manuscript is based on our original research and has neither been published, nor is being considered elsewhere for publication. Additionally, all the authors note that they do not have any relationships that they believe could be construed as a conflict of interest with regards to manuscript review process.

References

1. Wan GY, Liu Y, Chen BW, Liu YY, Wang YS, Zhang N. Recent advances of sonodynamic therapy in cancer treatment. *Cancer Biol Med* 2016;**13**:325−38.
2. Yang Y, Tu J, Yang D, Raymond JL, Roy RA, Zhang D. Photo- and sono-dynamic therapy: a review of mechanisms and considerations for pharmacological agents used in therapy incorporating light and sound. *Curr Pharm Des* 2019;**25**:401−12.
3. Costley D, Mc Ewan C, Fowley C, McHale AP, Atchison J, Nimikou N, et al. Treating cancer with sonodynamic therapy: a review. *Int J Hyperthermia Off J Eur Soc Hyperthermic Oncol North Am Hyperth Group* 2015;**31**:107−17.
4. Sadanala KC, Chaturvedi PK, Seo YM, Kin JM, Jo YS, Lee YK, et al. Sono-photodynamic combination therapy: a review on sensitizers. *Anticancer Res* 2014;**34**:4657−64.
5. Zheng Y, Ye J, Li Z, Chen H, Gao Y. Recent progress in sono-photodynamic cancer therapy: from developed new sensitizers to nanotechnology-based efficacy-enhancing strategies. *Acta Pharm Sin B* 2021;**11**:2197−219.
6. Shi X, Zhang CY, Gao J, Wang Z. Recent advances in photodynamic therapy for cancer and infectious diseases. *Wiley Interdiscip Rev Nanomed Nanobiotechnol* 2019;**11**:e1560.
7. McHale AP, Callan JF, Nomikou N, Fowley C, Callan B. Sonodynamic therapy: concept, mechanism and application to cancer treatment. *Therapeutic Ultrasound* 2016:429−50.
8. Wysocki M, Czarczynska-Goslinska B, Ziental D, Michalak M, Güzel E, Sobotta L. Excited state and reactive oxygen species against cancer and pathogens: a review on sonodynamic and sono-photodynamic therapy. *ChemMedChem* 2022;**17**:e202200185.
9. Li R, Chen Z, Dai Z, Yu Y. Nanotechnology assisted photo- and sonodynamic therapy for overcoming drug resistance. *Cancer Biol Med* 2021;**18**:388−400.
10. Nowak KM, Schwartz MR, Breza VR, Price RJ. Sonodynamic therapy: rapid progress and new opportunities for non-invasive tumor cell killing with sound. *Cancer Let* 2022;**532**:215592.
11. Rengeng L, Qianyu Z, Yuehong L, Zhongzhong P, Libo L. Sonodynamic therapy, a treatment developing from photodynamic therapy. *Photodiagnosis Photodyn Ther* 2017;**19**:159−66.
12. Gong Z, Dai Z. Design and challenges of sonodynamic therapy system for cancer theranostics: from equipment to sensitizers. *Adv Sci* 2021;**8**:2002178.
13. Zhou Y, Wang M, Dai Z. The molecular design of and challenges relating to sensitizers for cancer sonodynamic therapy. *Mater Chem Front* 2020;**4**:2223−34.
14. Roguin LP, Chiarante N, García Vior MC, Marino J. Zinc(II) phthalocyanines as photosensitizers for antitumor photodynamic therapy. *Int J Biochem Cell Biol* 2019;**114**:105575.
15. Janas K, Boniewska-Bernacka E, Dyrda G, Słota R. Porphyrin and phthalocyanine photosensitizers designed for targeted photodynamic therapy of colorectal cancer. *Bioorg Med Chem* 2021;**30**:115926.
16. Dubinina TV, Tomilova LG, Zefirov NS. Synthesis of phthalocyanines with an extended system of -electron conjugation. *Russ Chem Rev* 2013;**82**:865.
17. Breloy L, Yavuz O, Yilmaz I, Yagci Y, Versace DL. Design, synthesis and use of phthalocyanines as a new class of visible-light photoinitiators for free-radical and cationic polymerizations. *Polym Chem* 2021;**12**:4291−316.
18. Galstyan A. Turning photons into drugs: phthalocyanine-based photosensitizers as efficient photoantimicrobials. *Chem Eur J* 2021;**27**:1903−20.
19. Ragoussi ME, Torres T. Modern synthetic tools toward the preparation of sophisticated phthalocyanine-based photoactive systems. *Chem Asian* 2014;**9**:2676−707.
20. Singh VK, Kanaparthi RK, Giribabu L. Emerging molecular design strategies of unsymmetrical phthalocyanines for dye-sensitized solar cell applications. *RSC Adv* 2014;**4**:6970−84.
21. Jiang Z, Shao J, Yang T, Wang J, Jia L. Pharmaceutical development, composition and quantitative analysis of phthalocyanine as the photosensitizer for cancer photodynamic therapy. *J Pharm Biomed Anal* 2014;**87**:98−104.
22. Santos KLM, Barros RM, da Silva Lima DP, Nunes AMA, Sato MR, Faccio R, et al. Prospective application of phthalocyanines in the

photodynamic therapy against microorganisms and tumor cells: a mini-review. *Photodiagnosis Photodyn Ther* 2020;**32**:102032.
23. Swamy PCA, Sivaraman G, Priyanka RN, Raja SO, Ponnuvel K, Shanmugpriya J, et al. Near Infrared (NIR) absorbing dyes as promising photosensitizer for photo dynamic therapy. *Coord Chem Rev* 2020;**411**:213233.
24. Lo PC, Rodríguez-Morgade MS, Pandey RK, Ng DKP, Torres T, Dumoulin F. The unique features and promises of phthalocyanines as advanced photosensitisers for photodynamic therapy of cancer. *Chem Soc Rev* 2020;**49**:1041−56.
25. Han X, Wang Z, Shen M, Liu J, Li Z, Jia T, et al. A highly efficient organic solar energy-absorbing material based on phthalocyanine derivative for integrated water evaporation and thermoelectric power generation application. *J Mater Chem A* 2021;**9**:24452−9.
26. Huang Y, Qiu F, Chen R, Yan D, Zhu X. Fluorescence resonance energy transfer-based drug delivery systems for enhanced photodynamic therapy. *J Mater Chem B* 2020;**8**:3772−88.
27. Zhu TC, Finlay JC. The role of photodynamic therapy (PDT) physics. *Med Phys* 2008;**35**:3127−36.
28. Dąbrowski JM, Pucelik B, Regiel-Futyra A, Brindell M, Mazuryk O, Kyzioł A, et al. Engineering of relevant photodynamic processes through structural modifications of metallotetrapyrrolic photosensitizers. *Coord Chem Rev* 2016;**325**:67−101.
29. Hoshi T, Kobayashi N. Spectroscopic and structural properties of phthalocyanines deduced from their frontier molecular orbitals (MOs) and MO calculations. *Coord Chem Rev* 2017;**345**:31−41.
30. Wang M, Ishii K. Photochemical properties of phthalocyanines with transition metal ions. *Coord Chem Rev* 2022;**468**:214626.
31. McEwan C, Nesbitt H, Nicholas D, Kavanagh ON, McKenna K, Loan P, et al. Comparing the efficacy of photodynamic and sonodynamic therapy in non-melanoma and melanoma skin cancer. *Bioorg Med Chem* 2016;**24**:3023−8.
32. Liao S, Cai M, Zhu R, Fu T, Du Y, Kong J, et al. Antitumor effect of photodynamic therapy, sonodynamic therapy, sono-photodynamic therapy of chlorin e6 and other applications. *Mol Pharm* 2023;**20**:875−85.
33. Yan P, Liu LH, Wang P. Sonodynamic therapy (sdt) for cancer treatment: advanced sensitizers by ultrasound activation to injury tumor. *ACS Appl Bio Mater* 2020;**3**:3456−75.
34. Qian X, Zheng Y, Chen Y. Micro.nanoparticle-augmented sonodynamic therapy (sdt): breaking the depth shallow of photoactivation. *Adv Mater* 2016;**28**:8097−129.
35. Yumita N, Iwase Y, Watanabe T, Nishi K, Kuwahara H, Shigeyama M, et al. Involvement of reactive oxygen species in the enhancement of membrane lipid peroxidation by sonodynamic therapy with functionalized fullerenes. *Anticancer Res* 2014;**34**:6481−7.
36. Zhang Q, Bao C, Cai X, Jin L, Sun L, Lang Y, et al. Sonodynamic therapy-assisted immunotherapy: a novel modality for cancer treatment. *Cancer Sci* 2018;**109**:1330−45.
37. Tian J, Huang B, Nawaz MH, Zhang W. Recent advances of multi-dimensional porphyrin-based functional materials in photodynamic therapy. *Coord Chem Rev* 2020;**420**:213410.
38. Dąbrowski JM. Chapter Nine−Reactive oxygen species in photodynamic therapy: mechanisms of their generation and potentiation. *Adv Inorg Chem* 2017;**70**:343−94.
39. Zheng BD, He QX, Li X, Yoon J, Huang JD. Phthalocyanines as contrast agents for photothermal therapy. *Coord Chem Rev* 2021;**426**:213548.
40. Rak J, Pouckova P, Benes J, Vetvicka D. Drug delivery systems for phthalocyanines for photodynamic therapy. *Anticancer Res* 2019;**39**:3323−39.
41. Trendowski M. The promise of sonodynamic therapy. *Cancer Metastasis Rev* 2014;**33**:143−60.
42. Choi V, Rajora MA, Zheng G. Activating Drugs with sound: mechanisms behind sonodynamic therapy and the role of nanomedicine. *Bioconjug Chem* 2020;**31**:967−89.
43. Canavese G, Ancona A, Racca L, Canta M, Dumontel B, Barbaresco F, et al. Nanoparticle-assisted ultrasound: a special focus on sonodynamic therapy against cancer. *Chem Eng J* 2018;**340**:155−72.
44. Yamaguchi T, Kitahara S, Kusuda K, Okamoto J, Horise Y, Masamune K, et al. Current landscape of sonodynamic therapy for treating cancer. *Cancers* 2021;**13**:24.
45. Canaparo R, Foglietta F, Barbero N, Serpe L. The promising interplay between sonodynamic therapy and nanomedicine. *Adv Drug Deliv Rev* 2022;**189**:114495.
46. Giuntini F, Foglietta F, Marucco AM, Troia A, Dezhkunov NV, Pozzoli A, et al. Insight into ultrasound-mediated reactive oxygen species generation by various metal-porphyrin complexes. *Free Radic Biol Med* 2018;**121**:190−201.
47. Sazgarnia A, Shanei A, Eshghi H, Hassanzadeh-Khayyat M, Esmaily H, Shanei MM. Detection of sonoluminescence signals in a gel phantom in the presence of protoporphyrin IX conjugated to gold nanoparticles. *Ultrasonics* 2013;**53**:29−35.
48. Lacerda Q, Tantawi M, Leeper DB, Wheatley MA, Eisenbrey J. Emerging applications of ultrasound contrast agents in radiation therapy. *Ultrasound Med Biol* 2021;**47**:1465−74.
49. Dhaliwal A, Zheng G. Improving accessibility of EPR-insensitive tumor phenotypes using EPR-adaptive strategies: designing a new perspective in nanomedicine delivery. *Theranostics* 2019;**9**:8091−108.
50. Helfield B, Chen X, Watkins SC, Villanueva FS. Biophysical insight into mechanisms of sonoporation. *Proc Natl Acad Sci USA* 2016;**113**:9983−8.
51. Song L, Hou X, Wong KF, Yang Y, Qiu Z, Wu Y, et al. Gas-filled protein nanostructures as cavitation nuclei for molecule-specific sonodynamic therapy. *Acta Biomater* 2021;**136**:533−45.
52. Mehier-Humbert S, Bettinger T, Yan F, Guy RH. Plasma membrane poration induced by ultrasound exposure: implication for drug delivery. *J Control Release* 2005;**104**:213−22.
53. Güzel E, Günsel A, Bilgiçli AT, Atmaca GY, Erdoğmuş A, Yarasir MN. Synthesis and photophysicochemical properties of novel thiadiazole-substituted zinc (II), gallium (III) and silicon (IV) phthalocyanines for photodynamic therapy. *Inorganica Chim Acta* 2017;**467**:169−76.
54. Chen Y, Li L, Chen W, Chen H, Yin J. Near-infrared small molecular fluorescent dyes for photothermal therapy. *Chin Chem Lett* 2019;**30**:1353−60.
55. Özceşmeci İ, Gelir A, Gül A. Synthesis and photophysical properties of indium(III) phthalocyanine derivatives. *J Lumin* 2014;**147**:141−6.
56. Britton J, Martynov AG, Oluwole DO, Gorbunova YG, Tsivadze AY, Nyokong T. Improvement of nonlinear optical properties of phthalocyanine bearing diethyleneglycole chains: influence of symmetry lowering *vs* heavy atom effect. *J Porphyr Phthalocyanines* 2016;**20**:1296−305.
57. Güzel E, Atmaca GY, Kuznetsov AE, Turkkol A, Bilgin MD, Erdoğmuş A. Ultrasound *versus* light: exploring photophysicochemical and sonochemical properties of phthalocyanine-based therapeutics, theoretical study, and *in vitro* evaluations. *ACS Appl Bio Mater* 2022;**5**:1139−50.
58. Karanlik CC, Aguilar-Galindo F, Sobatta L, Güzel E, Erdoğmuş A. Combination of light and ultrasound: exploring sono−photochemical activities of phthalocyanine-based sensitizers. *J Phys Chem C* 2023;**127**:9145−53.
59. Granados-Tavera K, Zambrano-Angulo M, Montenegro-Pohlhammer N, Atmaca GY, Sobotta L, Güzel E, et al. Synergistic effect of ultrasound and light to efficient singlet oxygen formation for photodynamic purposes. *Dyes Pigments* 2023;**210**:110986.
60. Atmaca GY. Synthesis of palladium phthalocyanine and investigation of sono-photodynamic therapy properties. *CBUJOS* 2020;**16**:367−72.
61. Atmaca GY. Investigation of the differences between sono-photochemical and photochemical studies for singlet oxygen generation of indium phthalocyanine. *Inorganica Chim Acta* 2021;**515**:120052.

62. Sindelo A, Kobayashi N, Kimura M, Nyokong T. Physicochemical and photodynamic antimicrobial chemotherapy activity of morpholine-substituted phthalocyanines: effect of point of substitution and central metal. *J Photochem Photobiol Chem* 2019;**374**:58−67.
63. Yamamoto S, Kurobayshi K, Murakami TN, Kwon E, Stillman M, Kobayashi N, et al. Regioregular phthalocyanines substituted with bulky donors at non-peripheral positions. *Chem Eur J* 2017;**23**:15446−54.
64. Ikeuchi T, Mack J, Nyokong T, Kobayashi N, Kimura M. Aggregation control of robust water-soluble zinc(ii) phthalocyanine-based photosensitizers. *Langmuir ACS J Surf Colloids* 2016;**32**:11980−5.
65. Farajzadeh N, Atmaca GY, Erdoğmuş A, Koçak MB. Comparatively singlet oxygen efficiency by sono-photochemical and photochemical studies of new lutetium (III) phthalocyanines. *Dyes Pigments* 2021;**190**:109325.
66. Iwase Y, Yumita N, Nishi K, Kuwahara H, Fukai T, Ikeda FS, et al. Apoptosis induction by aluminum phthalocyanine tetrasulfonate-based sonodynamic therapy in HL-60 cells. *Jpn J Appl Phys* 2016;**54**:07HD05.
67. Bilgin MD, Aksel M, Degirmenci EH, Girit OB, Ozmen A. Efficacy of methylene blue and aliminium phthalocyanine mediated sono-photodynamic therapy on prostate cancer cell lines. *Biophys J* 2017;**112**:282a−3a.
68. Osaki T, Yokoe I, Uto Y, Ishizuka M, Tanaka T, Yamanaka N, et al. Bleomycin enhances the efficacy of sonodynamic therapy using aluminum phthalocyanine disulfonate. *Ultrason Sonochem* 2016;**28**:161−8.
69. Mack J, Kobayashi N. Low symmetry phthalocyanines and their analogues. *Chem Rev* 2011;**111**:281−321.
70. Dube E, Nwaji N, Mack J, Nyokong T. The photophysicochemical behavior of symmetric and asymmetric zinc phthalocyanines, surface assembled onto gold nanotriangles. *New J Chem* 2018;**42**:14290−9.
71. Göl C, Malkoç M, Yeşilot S, Durmuş M. Novel zinc(II) phthalocyanine conjugates bearing different numbers of BODIPY and iodine groups as substituents on the periphery. *Dyes Pigments* 2014;**111**:81−90.
72. Günsel A, Mutlu N, Atmaca GY, Günsel H, Bilgiçli AT, Erdoğmuş A, et al. Novel graphene oxide.zinc phthalocyanine composites bearing 3-chloro-4-fluorophenoxy: potential usage for sono.photochemical applications. *Chem Select* 2023;**8**:e202204546.
73. Karanlık CC, Atmaca GY, Erdoğmuş A. Improved singlet oxygen yields of new palladium phthalocyanines using sonochemistry and comparisons with photochemistry. *Polyhedron* 2021;**206**:115351.
74. Atmaca GY, Karanlık CC, Erdoğmuş A. Measurement of improved singlet oxygen generations of indium chloride phthalocyanines by comparatively sono-photochemical and photochemical studies. *Dyes Pigments* 2021;**194**:109630.
75. Atmaca GY, Karanlık CC, Erdoğmuş A. Novel silicon phthalocyanines with improved singlet oxygen generation by Sono-photochemical applications. *J Photochem Photobiol Chem* 2023;**436**:114365.
76. Pucelik B, Gürol I, Ahsen V, Dumoulin F, Dąbrowski JM. Fluorination of phthalocyanine substituents: improved photoproperties and enhanced photodynamic efficacy after optimal micellar formulations. *Eur J Med Chem* 2016;**124**:284−98.
77. Yu X, Lai S, Xin S, Chen S, Zhang X, She X, et al. Coupling of iron phthalocyanine at carbon defect site *via* $\pi-\pi$ stacking for enhanced oxygen reduction reaction. *Appl Catal B Environ* 2021;**280**:119437.
78. Mativetsky JM, Wang H, Lee SS, Whittaker-Brooks L, Loo YL. Face-on stacking and enhanced out-of-plane hole mobility in graphene-templated copper phthalocyanine. *Chem Commun* 2014;**50**:5319−21.
79. Kim SH, Namgoong JW, Yuk SB, Kim JY, Lee W, Chun Y, et al. Synthesis and characteristics of metal-phthalocyanines zhaotetra-substituted at non-peripheral (α) or peripheral (β) positions, and their applications in LCD color filters. *J Incl Phenom Macrocycl Chem* 2015;**82**:195−202.
80. Tillo A, Stolarska M, Kryjewski M, Popenda L, Sobotta L, Jurga S, et al. Phthalocyanines with bulky substituents at non-peripheral positions−synthesis and physico-chemical properties. *Dyes Pigments* 2016;**127**:110−5.
81. van de Winckel E, David B, Simoni MM, Gonzalez-Delgado JA, de la Escosura A, Cunha A, et al. Octacationic and axially di-substituted silicon (IV) phthalocyanines for photodynamic inactivation of bacteria. *Dyes Pigments* 2017;**145**:239−45.
82. Bıyıklıoğlu Z. Non-aggregated and water soluble amphiphilic silicon phthalocyanines with two axial substituents and their electrochemical properties. *Polyhedron* 2013;**63**:1−8.
83. Ünlü S, Elmalı FT, Atmaca GY, Erdoğmuş A. Synthesis of axially Schiff base new substituted silicon phthalocyanines and investigation of photochemical and sono-photochemical properties. *Photodiagnosis Photodyn Ther* 2022;**40**:103192.
84. Karanlık CC, Atmaca GY, Erdoğmuş A. Comparison of singlet oxygen production of ethyl vanillin substituted silicon phthalocyanine using sonophotodynamic and photodynamic methods. *J Mol Struct* 2023;**1274**:134498.
85. Kose GG, Karaoglan GK. Synthesis of a novel axially substituted silicon phthalocyanine sensitizer for efficient singlet oxygen generation by comparing PDT and SPDT studies. *Chem Phys* 2023;**565**:111737.
86. Atmaca GY. Measurement of singlet oxygen generation of 9(hydroxymethyl)anthracene substituted silicon phthalocyanine by sono-photochemical and photochemical studies. *J Mol Struct* 2021;**1226**:129320.
87. Atmaca GY. Investigation of singlet oxygen efficiency of di-axially substituted silicon phthalocyanine with sono-photochemical and photochemical studies. *Polyhedron* 2021;**193**:114894.
88. Ünlü S, Atmaca GY, Elmalı FT, Erdoğmuş A. Comparing singlet oxygen generation of schiff base substituted novel silicon phthalocyanines by sonophotochemical and photochemical applications. *Photochem Photobiol* 2023.
89. Atmaca GY, Aksel M, Keskin B, Bilgin MD, Erdoğmuş A. The photo-physicochemical properties and *in vitro* sonophotodynamic therapy activity of Di-axially substituted silicon phthalocyanines on PC3 prostate cancer cell line. *Dyes Pigments* 2021;**184**:108760.
90. Atmaca GY, Aksel M, Bilgin MD, Erdoğmuş A. Comparison of sonodynamic, photodynamic and sonophotodynamic therapy activity of fluorinated pyridine substituted silicon phthalocyanines on PC3 prostate cancer cell line. *Photodiagnosis Photodyn Ther* 2023;**42**:103339.
91. Zhao PH, Wu YL, Li XY, Feng LL, Zhang L, Zheng BY, et al. Aggregation-enhanced sonodynamic activity of phthalocyanine-artesunate conjugates. *Angew Chem Int Ed Engl* 2022;**61**:e202113506.
92. Günsel A, Alici EH, Bilgiçli AT, Arabaci G, Yarasi MN. Antioxidant properties of water-soluble phthalocyanines containing quinoline5-sulfonic acid groups. *Turk J Chem* 2019;**43**:1030−9.
93. Günsel A, Bilgiçli AT, Barut B, Taslimi P, Ozel A, Gülçin I, et al. Synthesis of water soluble tetra-substituted phthalocyanines: investigation of DNA cleavage, cytotoxic effects and metabolic enzymes inhibition. *J Mol Struc* 2020;**1214**:128210.
94. Simelane NWN, Matlou GG, Abrahamse H. Photodynamic therapy of aluminum phthalocyanine tetra sodium 2-mercaptoacetate linked to PEGylated copper−gold bimetallic nanoparticles on colon cancer cells. *Int J Mol Sci* 2023;**24**:1902.
95. Lu L, Lv F, Cao B, He X, Liu T. Saccharide substituted zinc phthalocyanines: optical properties, interaction with bovine serum albumin and near infrared fluorescence imaging for sentinel lymph nodes. *Molecules* 2014;**19**:523−37.
96. Çolak S, Durmuş M, Yıldız SZ. Investigation of the photophysical and photochemical properties of peripherally tetra-substituted water-soluble zwitterionic and cationic zinc(ii) phthalocyanines. *Dalton Trans* 2016;**45**:10402−10.
97. Li M, Mai B, Wang A, Wang X, Liu X, Song S, et al. Photodynamic antimicrobial chemotherapy with cationic phthalocyanines against

Escherichia coli planktonic and biofilm cultures. *RSC Adv* 2017;**7**:40734−44.
98. Çakır D, Çakır V, Bıyıklıoğlu Z, Durmuş M, Kantekin H. New water soluble cationic zinc phthalocyanines as potential for photodynamic therapy of cancer. *J Organomet Chem* 2013;**745**−**746**:423−31.
99. Neves LFF, Krais JJ, Rite BDV, Ramesh R, Resasco DE, Harrison RG. Targeting single-walled carbon nanotubes for the treatment of breast cancer using photothermal therapy. *Nanotechnology* 2013;**24**:375104.
100. Desai TJ, Toombs JE, Minna JD, Brekken RA, Udugamasooriya DG. Identification of lipid-phosphatidylserine (PS) as the target of unbiasedly selected cancer specific peptide-peptoid hybrid PPS1. *Oncotarget* 2016;**7**:30678−90.
101. Hu Q, Gao M, Feng G, Liu B. Mitochondria-targeted cancer therapy using a light-up probe with aggregation-induced-emission characteristics. *Angew Chem Int Ed* 2014;**53**:14225−9.
102. Liu Y, Zhang J, Tu Y, Zhu L. Potential-independent intracellular drug delivery and mitochondrial targeting. *ACS Nano* 2022;**16**:1409−20.
103. Zinovkin R, Zamyatnin A. Mitochondria-targeted drugs. *Curr Mol Pharmacol* 2019;**12**:202−14.
104. Wang R, Li X, Yoon J. Organelle-targeted photosensitizers for precision photodynamic therapy. *ACS Appl Mater Interfaces* 2021;**13**:19543−71.
105. Nene LC, Nyokong T. The in-vitro proliferation-suppression of MCF-7 and HeLa cell lines mediated by differently substituted ionic phthalocyanines in sonodynamic therapy supplemented-photodynamic therapy. *J Inorg Biochem* 2023;**239**:112084.
106. Çakır V, Çakır D, Göksel M, Durmuş M, Bıyıklıoğlu Z, Kantekin H. Synthesis, photochemical, bovine serum albumin and DNA binding properties of tetrasubstituted zinc phthalocyanines and their water soluble derivatives. *J Photochem Photobiol Chem* 2015;**299**:138−51.
107. Liu S, Ma J, Xue EY, Wang S, Zheng Y, Ng DKP, et al. Polymeric phthalocyanine-based nanosensitizers for enhanced photodynamic and sonodynamic therapies. *Adv Healthc Mater* 2023;**12**:e2300481.
108. Karaoğlan G. Synthesis of a novel zinc phthalocyanine with peripherally coordinated Ru(II) complexes; sono-photochemical, photochemical and photophysical studies. *J Mol Struct* 2022;**1261**:132886.
109. Atmaca GY, Elmalı FT, Erdoğmuş A. Improved singlet oxygen generation of axially ruthenium(II) complex substituted silicon(IV) phthalocyanine by sono-photochemical studies. *J Mol Struct* 2023;**1274**:134332.
110. Bakhshizadeh M, Moshirian T, Esmaily H, Rajabi O, Nassirli H, Sazgarnia A. Sonophotodynamic therapy mediated by liposomal zinc phthalocyanine in a colon carcinoma tumor model: role of irradiating arrangement. *Iran J Basic Med Sci* 2017;**20**:1088−92.
111. Martins YA, Fonseca MJV, Pavan TZ, Lopez RFV. Bifunctional therapeutic application of low-frequency ultrasound associated with zinc phthalocyanine-loaded micelles. *Int J Nanomedicine* 2020;**15**:8075−95.
112. Gong Y, Wang X, Gong F, Li G, Yang Y, Hou L, et al. Phthalocyanine iron nanodots for combined chemodynamic-sonodynamic cancer therapy. *Sci China Mater* 2022;**65**:2600−8.
113. Nene LC, Nyokong T. Photo-sonodynamic combination activity of cationic morpholino-phthalocyanines conjugated to nitrogen and nitrogen-sulfur doped graphene quantum dots against MCF-7 breast cancer cell line *in vitro*. *Photodiagnosis Photodyn Ther* 2021;**36**:102573.
114. Nene LC, Nyokong T. Enhancement of the in vitro anticancer photo-sonodynamic combination therapy activity of cationic thiazole-phthalocyanines using gold and silver nanoparticles. *J Photochem Photobiol Chem* 2023;**435**:114339.
115. Xu HN, Chen HJ, Zheng BY, Zheng YQ, Ke MR, Huang JD. Preparation and sonodynamic activities of water-soluble tetra-α-(3-carboxyphenoxyl) zinc(II) phthalocyanine and its bovine serum albumin conjugate. *Ultrason Sonochem* 2015;**22**:125−31.
116. Yin T, Yin J, Ran H, Ren Y, Lu C, Liu L, et al. Hypoxia-alleviated sonodynamic therapy based on a hybrid protein oxygen carrier to enhance tumor inhibition. *Biomater Sci* 2021;**10**:294−305.
117. Li D, Pan J, Xu S, Cheng B, Wu S, Dai Q, et al. Programmable phthalocyanine-iron-based nanoreactor for fluorescence.magnetic resonance dual-modality imaging-guided sono.chemodynamic therapies. *Chem Eng J* 2023;**452**:139330.
118. Nyokong T, Antunes E. Influence of nanoparticle materials on the photophysical behavior of phthalocyanines. *Coord Chem Rev* 2013;**257**:2401−18.
119. Dang Y, Guan J. Nanoparticle-based drug delivery systems for cancer therapy. *Smart Mater Med* 2020;**1**:10−9.
120. Azzi S, Hebda J, Gavard J. Vascular permeability and drug delivery in cancers. *Front Oncol* 2013;**3**:231.
121. Shenoy AK, Lu J. Cancer cells remodel themselves and vasculature to overcome the endothelial barrier. *Cancer Lett* 2016;**380**:534−44.
122. Nel A, Ruoslahti E, Meng H. New insights into "permeability" as in the enhanced permeability and retention effect of cancer nanotherapeutics. *ACS Nano* 2017;**11**:9567−9.
123. Kalyane D, Raval N, Maheshwari R, Tambe V, Kalia K, Tekade RK. Employment of enhanced permeability and retention effect (EPR): nanoparticle-based precision tools for targeting of therapeutic and diagnostic agent in cancer. *Mater Sci Eng C* 2019;**98**:1252−76.
124. Wu J. The enhanced permeability and retention (EPR) effect: the significance of the concept and methods to enhance its application. *J Pers Med* 2021;**11**:8.
125. Yyildirim A, Shi D, Roy S, Blum NT, Chattaraj R, Cha JN, et al. Nanoparticle-mediated acoustic cavitation enables high intensity focused ultrasound ablation without tissue heating. *Appl Mater Interfaces* 2018;**10**:36786−95.
126. Yildirim A, Chattaraj R, Blum NT, Goodwin AP. Understanding acoustic cavitation initiation by porous nanoparticles: toward nanoscale agents for ultrasound imaging and therapy. *Chem Mater Publ Am Chem Soc* 2016;**28**:5962−72.
127. Shanei A, Shanei MM. Effect of gold nanoparticle size on acoustic cavitation using chemical dosimetry method. *Ultrason Sonochem* 2017;**34**:45−50.
128. Achadu OJ, Nyokong T. Graphene quantum dots decorated with maleimide and zinc tetramaleimido-phthalocyanine: application in the design of "OFF-ON" fluorescence sensors for biothiols. *Talanta* 2017;**166**:15−26.
129. Oluwole DO, Nwaji N, Nene LC, Mokone L, Dube E, Nyokong T. Novel nano-dyad of homoleptic sandwich-type phthalocyanines with nitrogen doped graphene quantum dots for nonlinear optics. *New J Chem* 2018;**42**:10124−33.
130. Dube E, Nwaji N, Oluwole DO, Mack J, Nyokong T. Investigation of photophysicochemical properties of zinc phthalocyanines conjugated to metallic nanoparticles. *J Photochem Photobiol Chem* 2017;**349**:148−61.
131. Dube E, Oluwole DO, Nwaji N, Nyokong T. Glycosylated zinc phthalocyanine-gold nanoparticle conjugates for photodynamic therapy: effect of nanoparticle shape. *Spectrochim Acta Mol Biomol Spectrosc* 2018;**203**:85−95.
132. Wang J, Jiao Y, Shao Y. Mesoporous silica nanoparticles for dual-mode chemo-sonodynamic therapy by low-energy ultrasound. *Materials* 2018;**11**:2041.
133. You DG, Deepagan VG, Um W, Jeon S, Son S, Chang H, et al. ROS-generating TiO_2 nanoparticles for non-invasive sonodynamic therapy of cancer. *Sci Rep* 2016;**6**:23200.
134. Luo J, Ca J, Ma G, Wang X, Sun Y, Zhang C, et al. Collagenase-Loaded H-TiO_2 Nanoparticles enhance ultrasound imaging-guided sonodynamic therapy in a pancreatic carcinoma xenograft model *via* digesting stromal barriers. *ACS Appl Mater Interfaces* 2022;**14**:40535−45.
135. Yumita N, Iwase Y, Umemura SI, Chen FS, Momose Y. Sonodynamically-induced anticancer effects of polyethylene glycol-modified carbon nano tubes 2020;**40**:2549−57.
136. Kim TH, Lee S, Chen X. Nanotheranostics for personalized medicine. *Expert Rev Mol Diagn* 2013;**13**:257−69.

137. Jo SD, Ku SH, Won YY, Kim SH, Kwon IC. Targeted nanotheranostics for future personalized medicine: recent progress in cancer therapy. *Theranostics* 2016;**6**:1362−77.
138. Zhang N, Xiong G, Liu Z. Toxicity of metal-based nanoparticles: challenges in the nano era. *Front Bioeng Biotechnol* 2022;**10**:1−16.
139. Ye W, Kruger K, Sanchez-Iglesias A, Garcia I, Jia X, Sutter J, et al. CTAB Stabilizes silver on gold nanorods. *Chem Mater* 2020;**32**: 1650−6.
140. Steckiewicz KP, Barcinska E, Sobczak K, Tomczyk E, Wojcik M, Inkielewicz-Stepniak I. Assessment of anti-tumor potential and safety of application of glutathione stabilized gold nanoparticles conjugated with chemotherapeutics. *Int J Med Sci* 2020;**17**: 824−33.
141. Shameer AB, Gunjan B, Rudrappa S, Subramania I, Vijayashree N. Comparative study of one pot synthesis of PEGylated gold and silver nanoparticles for imaging and radiosensitization of oral cancers. *Radiat Phys Chem* 2022;**194**:109990.
142. Matei I, Buta CM, Turcu IM, Culita D, Munteanu C, Ionita G. Formation and stabilization of gold nanoparticles in bovine serum albumin solution. *Molecules* 2019;**24**:3395.
143. Gounden S, Daniels A, Singh M. Chitosan-modified silver nanoparticles enhance cisplatin activity in breast cancer cells. *Biointergace Res Appl Chem* 2021;**11**:10572−84.
144. Dube E, Soy R, Shumba M, Nyokong T. Photophysicochemical behaviour of phenoxy propanoic acid functionalised zinc phthalocyanines when grafted onto iron oxide and silica nanoparticles: effects in photodynamic antimicrobial chemotherapy. *J Lumin* 2021; **234**:117939.
145. Pflieger R, Chave T, Vite G, Jouve L, Nikitenko SI. Effect of operational conditions on sonoluminescence and kinetics of H_2O_2 formation during the sonolysis of water in the presence of Ar.O2 gas mixture. *Ultrason Sonochem* 2015;**26**:169−75.
146. Wood RJ, Vévert C, Lee J, Bussemaker MJ. Flow effects on phenol degradation and sonoluminescence at different ultrasonic frequencies. *Ultrason Sonochem* 2020;**63**:104892.
147. Brotchie A, Grieser F, Ashokkumar M. Effect of power and frequency on bubble-size distributions in acoustic cavitation. *Phys Rev Lett* 2009;**102**:084302.
148. Merouani S, Hamdaoui O, Rezgui Y, Guemini M. Effects of ultrasound frequency and acoustic amplitude on the size of sonochemically active bubbles − theoretical study. *Ultrason Sonochem* 2013; **20**:815−9.
149. Misík V, Riesz P. Free radical intermediates in sonodynamic therapy. *Ann N Y Acad Sci* 2000;**899**:335−48.
150. Kessel D, Lo J, Jeffers R, Brian Fowlkes J, Cain C. Modes of photodynamic *vs* sonodynamic cytotoxicity. *J Photochem Photobiol, B* 1995;**28**:219−21.
151. Senapathy GJ, George BP, Abrahamse H. Enhancement of phthalocyanine mediated photodynamic therapy by catechin on lung cancer cells. *Molecules* 2020;**25**:21.
152. Chota A, George BP, Abrahamse H. Dicoma anomala enhances phthalocyanine mediated photodynamic therapy in mcf-7 breast cancer cells. *Front Pharmacol* 2022;**13**:892490.
153. Nkune NW, Kruger CA, Abrahamse H. Synthesis of a novel nanobioconjugate for targeted photodynamic therapy of colon cancer enhanced with cannabidiol. *Oncotarget* 2022;**13**:156−72.